NAVAL POSTGRADUATE SCHOOL

MONTEREY, CALIFORNIA

THESIS

ANALYSIS OF AN IMPROVED SOLAR-POWERED HYDROGEN GENERATION SYSTEM FOR SUSTAINED RENEWABLE ENERGY PRODUCTION

by

Sen Feng Yu

December 2017

Thesis Advisor:	Garth V. Hobson
Co-Advisor:	Andrea D. Holmes
Second Reader:	Anthony J. Gannon

Approved for public release. Distribution is unlimited.

THIS PAGE INTENTIONALLY LEFT BLANK

REPORT DOCUMENTATION PAGE	Form Approved OMB No. 0704–0188

Public reporting burden for this collection of information is estimated to average 1 hour per response, including the time for reviewing instruction, searching existing data sources, gathering and maintaining the data needed, and completing and reviewing the collection of information. Send comments regarding this burden estimate or any other aspect of this collection of information, including suggestions for reducing this burden, to Washington headquarters Services, Directorate for Information Operations and Reports, 1215 Jefferson Davis Highway, Suite 1204, Arlington, VA 22202-4302, and to the Office of Management and Budget, Paperwork Reduction Project (0704-0188) Washington, DC 20503.

1. AGENCY USE ONLY *(Leave blank)*	2. REPORT DATE December 2017	3. REPORT TYPE AND DATES COVERED Master's thesis

4. TITLE AND SUBTITLE
ANALYSIS OF AN IMPROVED SOLAR-POWERED HYDROGEN GENERATION SYSTEM FOR SUSTAINED RENEWABLE ENERGY PRODUCTION

5. FUNDING NUMBERS

6. AUTHOR(S) Sen Feng Yu

7. PERFORMING ORGANIZATION NAME(S) AND ADDRESS(ES)
Naval Postgraduate School
Monterey, CA 93943-5000

8. PERFORMING ORGANIZATION REPORT NUMBER

9. SPONSORING /MONITORING AGENCY NAME(S) AND ADDRESS(ES)
Office of Naval Research, Energy Systems Technology Evaluation Program (ESTEP), under technical monitoring of Stacey Curtis and Richard Carlin.

10. SPONSORING / MONITORING AGENCY REPORT NUMBER

11. SUPPLEMENTARY NOTES The views expressed in this thesis are those of the author and do not reflect the official policy or position of the Department of Defense or the U.S. Government. IRB number ____N/A____.

12a. DISTRIBUTION / AVAILABILITY STATEMENT
Approved for public release. Distribution is unlimited.

12b. DISTRIBUTION CODE

13. ABSTRACT (maximum 200 words)

The purpose of this thesis was to implement a data collection method to measure and characterize the performance of a renewable hydrogen generation system and improve the system reliability for continuous operation.

While the power consumption for the dehumidifiers was constant, the amount of water produced depended on the ambient condition. To produce enough water to meet electrolyzer demand, more dehumidifiers should be added. Water production using dehumidification accounted for the majority of the energy consumption. The electrolyzer demonstrated great flexibility in operating with intermittent power. As the power available increased, the amount of hydrogen produced increased, while the efficiency of the electrolyzer decreased. The fuel cell supplied power to a wide range of loads that were less than 100 W. Similar to the electrolyzer, as the fuel cell power output increased, efficiency decreased.

Hydrogen production using renewable energy has proved effective. Hydrogen produced was only used to generate electric power using a fuel cell, but other hydrogen-powered applications should also be considered to broaden the use of hydrogen within the Department of Defense. Lastly, other means of producing water should also be investigated to improve the overall efficiency of the hydrogen production system.

14. SUBJECT TERMS
renewable energy, water, dehumidifier, electrolysis, electrolyzer, hydrogen, PEM fuel cell, fuel cell, efficiency

15. NUMBER OF PAGES 91

16. PRICE CODE

17. SECURITY CLASSIFICATION OF REPORT	18. SECURITY CLASSIFICATION OF THIS PAGE	19. SECURITY CLASSIFICATION OF ABSTRACT	20. LIMITATION OF ABSTRACT
Unclassified	Unclassified	Unclassified	UU

NSN 7540–01-280-5500 Standard Form 298 (Rev. 2–89)
Prescribed by ANSI Std. 239–18

THIS PAGE INTENTIONALLY LEFT BLANK

Approved for public release. Distribution is unlimited.

ANALYSIS OF AN IMPROVED SOLAR-POWERED HYDROGEN GENERATION SYSTEM FOR SUSTAINED RENEWABLE ENERGY PRODUCTION

Sen Feng Yu
Lieutenant, United States Navy
B.S., University of California, Davis, 2008

Submitted in partial fulfillment of the
requirements for the degree of

MASTER OF SCIENCE IN MECHANICAL ENGINEERING

from the

NAVAL POSTGRADUATE SCHOOL
December 2017

Approved by: Garth V. Hobson
Thesis Advisor

Andrea D. Holmes
Co-Advisor

Anthony J. Gannon
Second Reader

Garth V. Hobson
Chair, Department of Mechanical and Aerospace Engineering

THIS PAGE INTENTIONALLY LEFT BLANK

ABSTRACT

The purpose of this thesis was to implement a data collection method to measure and characterize the performance of a renewable hydrogen generation system and improve the system reliability for continuous operation.

While the power consumption for the dehumidifiers was constant, the amount of water produced depended on the ambient condition. To produce enough water to meet electrolyzer demand, more dehumidifiers should be added. Water production using dehumidification accounted for the majority of the energy consumption. The electrolyzer demonstrated great flexibility in operating with intermittent power. As the power available increased, the amount of hydrogen produced increased, while the efficiency of the electrolyzer decreased. The fuel cell supplied power to a wide range of loads that were less than 100 W. Similar to the electrolyzer, as the fuel cell power output increased, efficiency decreased.

Hydrogen production using renewable energy has proved effective. Hydrogen produced was only used to generate electric power using a fuel cell, but other hydrogen-powered applications should also be considered to broaden the use of hydrogen within the Department of Defense. Lastly, other means of producing water should also be investigated to improve the overall efficiency of the hydrogen production system.

THIS PAGE INTENTIONALLY LEFT BLANK

TABLE OF CONTENTS

I. INTRODUCTION....1
- A. MOTIVATION....1
- B. LITERATURE REVIEW....3
  - 1. High Energy Density Batteries Storage System....4
  - 2. Pumped-Storage Hydroelectricity System....5
  - 3. Compressed Air Energy Storage System....6
  - 4. Hydrogen Energy Storage System....6
- C. PREVIOUS SETUP....7
  - 1. Electrical System....8
  - 2. Mechanical System....9

II. ENABLING TECHNOLOGY....11
- A. DEHUMIDIFICATION....11
- B. ELECTROLYSIS....12
- C. ELECTROCHEMICAL FUEL CELL....15

III. CURRENT SETUP....19
- A. SYSTEM RECONFIGURATION....19
  - 1. Electrical....19
  - 2. Mechanical/Plumbing....21
- B. AUTOMATED DATA COLLECTION METHOD....26
  - 1. Equipment....27
  - 2. Software....28
  - 3. Measurements....29

IV. RESULT AND DISCUSSION....31
- A. DEHUMIDIFIER....31
- B. ELECTROLYZER....33
- C. FUEL CELL....36
- D. SYSTEM EFFICIENCY....45
- E. SOLAR POWER TEST....49

V. CONCLUSION....55

VI. RECOMMENDATIONS....57
- A. AUTOMATED CONTROL SYSTEM....57
- B. OTHER WAYS OF WATER PRODUCTION....57

C. OTHER APPLICATION OF HYDROGEN 57

APPENDIX A. CALCULATIONS.....59

APPENDIX B. MATLAB CODE 61

APPENDIX C. DETAILED EXPERIMENTAL ELECTROLYZER RESULTS.....65

APPENDIX D. ELECTRICAL DIAGRAM.....67

APPENDIX E. MECHANICAL DIAGRAM 69

LIST OF REFERENCES 71

INITIAL DISTRIBUTION LIST 73

LIST OF FIGURES

Figure 1. Net Electricity Generation from Select Fuels. Source: [6]. 2

Figure 2. Energy Storage Portfolio in the United States in 2011. Source: [11]. 5

Figure 3. Previous Concept Design Diagram. Source: [14]. 8

Figure 4. Peltier Effect. Source: [16]. 12

Figure 5. Basic Scheme of an Alkaline Water Electrolyzer. Source: [17]. 13

Figure 6. Typical Polarization Curve for Low Temperature Electrolyzer Source: [18].....15

Figure 7. Basic Operations of a Fuel Cell. Source: [20]. 16

Figure 8. Typical Polarization Curve for Low Temperature Fuel Cell. Source: [20].....17

Figure 9. Picture of Solar Panels on the Roof 20

Figure 10. Solar Panel Reconfiguration 20

Figure 11. Picture of the System Before Consolidation 22

Figure 12. Shed Housing the Hydrogen Production Facility 22

Figure 13. Reconfigured Hydrogen Production Facility 23

Figure 14. Picture of Modified Dehumidifier Drain Port.....24

Figure 15. Plumbing One Line for Hydrogen Production System 25

Figure 16. Data Acquisition Components 28

Figure 17. Dehumidifier Energy Consumption Profile 31

Figure 18. Energy Consumption per Gram of Water vs Temperature Difference ($T_{drybulb} - T_{dewpoint}$).....32

Figure 19. Electrolyzer Current-Voltage Polarization Curve.....33

Figure 20. Power and Hydrogen Flowrate Ratio.....34

Figure 21. Electrolyzer Efficiency versus Input Power 36

Figure 22. Picture of Variable Resistor Used 37

Figure 23. Current-Voltage (IV) Polarization Curve H100 Fuel Cell 38

Figure 24. Fuel Cell Load Circuit 38

Figure 25. Fuel Cell Efficiency Curve 39

Figure 26. Picture of 3D Printed Oxygen Adapter 40

Figure 27. Fuel Cell Performance Comparison—with and without Oxygen Injection 41

Figure 28. Fuel Cell Performance Characteristics with 100W Lightbulb Load—Overall 42

Figure 29. Fuel Cell Performance Characteristics—Short-Circuit On 43

Figure 30. Fuel Cell Performance Loss with Short-Circuit Off 43

Figure 31. Fuel Cell Efficiency with Short-Circuit On 44

Figure 32. Fuel Cell Efficiency with Short-Circuit Off 45

Figure 33. Power Efficiency Process 46

Figure 34. Power Efficiency 47

Figure 35. Energy Efficiency Process 48

Figure 36. Energy Efficiency 49

Figure 37. Hydrogen Production with Solar Power—without Electrolyzer Current Control 50

Figure 38. Hydrogen Production with Solar Power—with Electrolyzer Current Control 52

Figure 39. Solar Power Available and Solar Power Consumed 54

LIST OF TABLES

Table 1. Three Categories of Energy Storage. Adapted from [9]. 4

Table 2. Main Components of LT Aviles' System 10

Table 3. Summaries of Measurement Taken 29

Table 4. Water Produced by Dehumidifier on Different Dates 32

Table 5. Solar Power Experimental Results.....52

THIS PAGE INTENTIONALLY LEFT BLANK

LIST OF ACRONYMS AND ABBREVIATIONS

AEMR	Annual Energy Management Report
BTU	British Thermal Units
DC	Direct Current
DOD	Department of Defense
DOE	Department of Energy
EIA	Energy Information Administration
GW	Gigawatt
HES	Hydrogen Energy Storage
HVAC	Heating, Ventilation and Air Conditioning
LED	Light-Emitting Diode
LHV	Lower Heating Value
MW	Megawatt
MWh	Megawatt hour
NREL	National Renewable Energy Laboratory
PEM	Proton Exchange Membrane
PV	Photovoltaic
SLPM	Standard Liters Per Minute
SMES	Superconducting Magnetic Energy Storage
WHE	Weight Handling Equipment

THIS PAGE INTENTIONALLY LEFT BLANK

ACKNOWLEDGMENTS

I would like to thank Dr. Garth Hobson, Dr. Anthony Gannon, Ms. Andrea Holmes, and Mr. John Gibson for their support and guidance throughout the project. Also, I would like to thank LT Erik Desousa for his expertise in using the 3D printer. Lastly, I would like to thank my wife, Rachel, for her patience and support during my time in graduate school.

THIS PAGE INTENTIONALLY LEFT BLANK

I. INTRODUCTION

A. MOTIVATION

We are a society that depends heavily on the reliable delivery of electricity, and the Department of Defense (DOD) is no exception. The U.S. consumed 102,762 petajoules of energy in 2016, and 39% of the energy was used to produce electricity [1]. The DOD installations rely on electricity to support the critical missions of our warfighters and electricity use accounts for 50% of DOD installation energy [2]. The incorporation of computer networks' control of the electrical grid systems has improved grid efficiency and reliability because it allows grid operators to remotely monitor grid status and effectively identify signs of failure. However, the convenience of having remote monitors and control of field devices exposed the power grid to cyber-attacks. Our power grid is highly susceptible to our adversaries. "In 2014, Admiral Michael Rogers, director of the National Security Agency, testified before Congress that China and a few other countries are likely to possess the resources and capability to shut down the U.S. power grid" [3]. Even in the absence of malicious cyber attackers, our aging electric grid is experiencing an increasing number of major event day outages [4].

Currently, the DOD installations largely depend on local power companies to provide reliable electric power to support its missions. Without sufficient on-site generation, the installations are only as resilient as the resiliency of the power grid. Therefore, in an effort to enhance its energy resilience, the DOD is aggressively setting its renewable energy goals to increase onsite generation. According to Department of Defense Annual Energy Management Report (AEMR) in 2015, DOD had committed to deploy 3 gigawatts (GW) of renewable power on its installation by FY 2025 [2]. Renewable energy generation on board installations enhances mission assurance and improves installation resiliency because it reduces installations' dependency on off-site power grid. In addition, unlike traditional power generators or backup power, renewable energy generation does not depend on fossil fuels and reduces installations' dependency on fossil fuel infrastructures that are vulnerable to cyber and physical attacks.

Lastly, installing renewable generation on board DOD installations does not mean a premium price tag over traditional generation. Because of government incentives and market demand, the cost of renewable generation has been falling, particularly photovoltaic (PV) and wind generation. According to Lazard, the cost of PV decreased by 85% over the last seven years, and the levelized cost of photovoltaic plant, in terms of cost per megawatt hour (MWh), is comparable with traditional fossil fuel plants [5]. As the renewable technology continues to mature, it will only drive the capital cost down even further. This is one of the reasons why the Energy Information Administration (EIA) predicts that the renewable electricity generation will continue to rise as shown in Figure 1. Even though not entirely with renewable energy, some DOD installations are already self-sustaining with on-site generation. At the Marine Corps Air Ground Combat Center Twentynine Palms, two cogeneration plants along with PV can supply enough power to the base during winter months. Therefore, critical DOD installations may well be powered entirely with renewable energy in the near future.

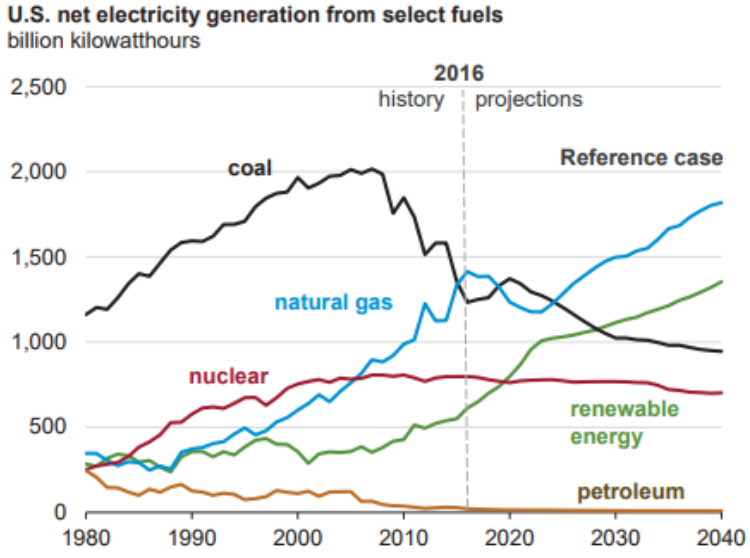

Figure 1. Net Electricity Generation from Select Fuels. Source: [6].

However, as renewable energy penetration within DOD installations increases, the need for energy storage also increases. Unlike traditional generation, renewable

generation, particularly wind and solar, is intermittent and do not generate power to match demand. The system can either over-generate or under-generate, depending on the demand because wind does not always blow and sun does not always shine when electricity is needed. When the system under-generates, demand can still be supplemented with traditional generation and does not pose a risk. However, when the system over-generates, it needs to be curtailed in the absence of an energy storage system to avoid damage to the grid. California has a solar penetration of 14.1% measured in MWh in 2016 [7]. For more than 30 days in January, February, and March of 2017, California had to pay Arizona to take the excess electricity it produced to avoid overloading its power lines [8]. Therefore, as renewable generation increases, the DOD needs to invest in energy storage systems to utilize excess generation.

B. LITERATURE REVIEW

The selection of an energy storage system is based on the criteria of discharge time and energy density, and there are three categories of applications: power quality, bridging power, and energy management [9]. Power quality applications are employed to provide transient stability and frequency regulation. These applications require rapid response, typically within a fraction of a second. Discharge time for this applications, is relatively short, up to about 10 minutes and requires continuous cycling. Flywheels, capacitors, and superconducting magnetic energy storage (SMES) are suitable for power quality applications [9]. Bridging power applications are employed as reserve to bridge the gap between generation and demand due to forecast uncertainty and unit commitment error. The response time for bridging power applications is relatively longer than power quality applications and ranges from seconds to minutes. Discharge times can be up to an hour and have less cycling than power quality applications. Several battery technologies, such as lead-acid, nickel-cadmium, nickel-metal hydride, and lithium-ion batteries, are suitable for bridging applications [9]. Energy management applications are employed to store energy at a time of low demand and discharge the energy at a time of high demand. These applications generally require a continuous discharge time of several hours or more. High energy density batteries, pumped hydro, compressed air, and hydrogen

energy storage are suitable for energy management applications [9]. Table 1 summarizes the three categories of energy storage applications.

Table 1. Three Categories of Energy Storage. Adapted from [9].

Category	**Discharge Time Required**	**Technology**
Power Quality	seconds to minutes	Flywheels, capacitors, and superconducting magnetic energy storage
Bridging Power	minutes to ~1 hour	batteries
Energy Management	hours	High-energy density batteries, pumped hydro, compressed air, and hydrogen energy storage

The DOD needs to invest in energy storage system that can be used to store excess energy generated and use it at a later time. The technologies suitable for energy management are reviewed: high energy density batteries, pumped-storage hydroelectricity, and hydrogen energy storage.

1. High Energy Density Batteries Storage System

High-density batteries are a new contender in the energy storage market. Prior to 2009, nine grid scale battery storage had been installed, totaling about 46 megawatt (MW) of rated power [10]. The technologies for those batteries are sodium based, nickel based or lead-acid based. Since then, the advancement of lithium ion technology has increased the utilization of batteries in grid scale energy storage systems. In 2015, 145 MW of grid scale lithium ion projects came online, which represented 95% of the total capacity installed for the year [10]. The lithium ion battery is favored over other batteries because of its high-energy density. With a nominal voltage of 3.7 V, it is much higher than many other batteries. That means fewer cells are needed to produce the same amount of power. In addition, lithium ion batteries have an efficiency of 85 to 95 percent and an expected lifetime of 10 to 15 years or 2,000 to 3,000 cycles [10].

2. Pumped-Storage Hydroelectricity System

Pumped hydroelectric storage is the oldest and most mature energy storage system. The first pumped hydroelectric plant came online in the 1920s in the United States [11]. Pumped hydroelectric plants use excess electricity during low demand and pump water from a lower altitude reservoir to an upper reservoir and store the energy as potential energy. During high demand, water is released from the reservoir to turn a water turbine and drive an electric generator to produce electricity. Both the energy and power density of pumped hydro plants depend on the elevation difference of the upper and lower reservoir or the head of the water. Therefore, to maximize the capacity of a pumped hydro plant, the site must have a high variation in topographic elevation. In addition, water must be available at the site or near the site that can be routed to the reservoir, which can cause environmental concern. The application of pumped hydroelectric plants is limited to large scale (+100 MW) and certain locations because of the specific geographic requirements. Due to the maturity and reliability of the system, pumped hydro is the primary energy storage system deployed in the United States. Currently, pumped hydro represents 98.9% of energy storage capacity in the United States, as shown in Figure 2.

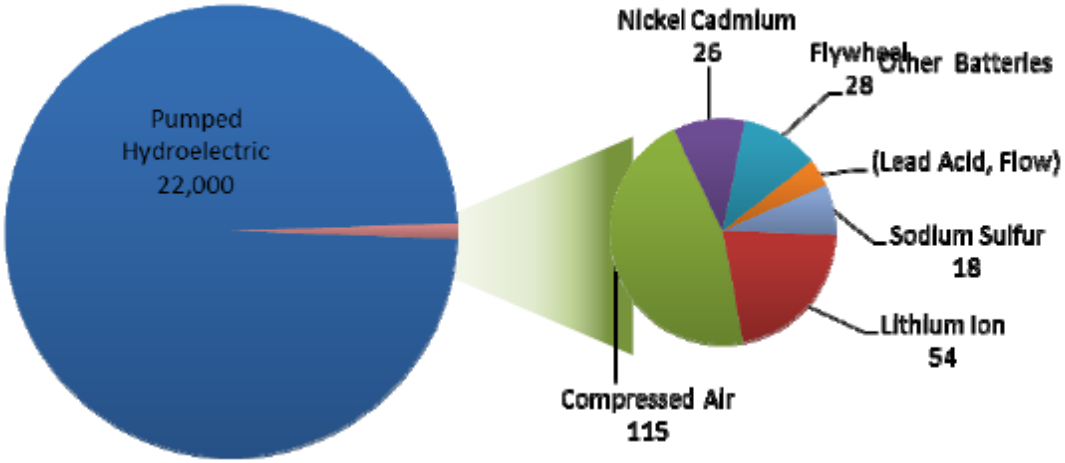

Figure 2. Energy Storage Portfolio in the United States in 2011. Source: [11].

3. Compressed Air Energy Storage System

Similar to pumped hydro, compressed air energy storage (CAES) compresses ambient air during times of low demand and stores it under pressure for use at times of high demand. The compressed air is usually stored in an underground cavern. When electricity is needed, the pressurized air is heated and run through a turbine that is connected to a generator to produce electricity. A CAES plant is practically like a conventional gas turbine plant. Instead of using the turbine work to compress the gas, which normally uses up to 2/3s of the turbine work [12], the gas is pre-compressed using other energy sources. Therefore, a CAES plant can produce 3 times the output when compared with a similar sized conventional gas turbine plant. However, specific geographic requirements limit deployment. Preferred locations are in artificially constructed salt caverns in deep salt formations [12]. Only one 110 MW CAES plant exists in the United States, and it is located in McIntosh, Alabama [11]. Another limitation of a CAES plant is its use of fossil fuel to heat the air before it enters the turbine if there is no thermal storage system installed to capture the heat produced during the compression process.

4. Hydrogen Energy Storage System

Hydrogen energy storage is an emergent technology that is receiving more interest as a deployable method to store excess renewable power generation. Hydrogen can be produced with renewable energy through electrolysis, thermochemical conversion of biomass, photolytic and fermentative micro-organism systems, photoelectrochemical systems, and high-temperature chemical cycle water splitting [13]. Consumed directly as a fuel, hydrogen can be converted back to grid electricity through either a fuel cell or a combustion engine. Hydrogen can also be used directly to power fuel cell vehicles and material handling equipment. Lastly, due to its high-energy density, hydrogen is also being deployed on drones to extend range or fly time. In 2014, National Renewable Energy Laboratory (NREL) hosted a conference with industry experts to deliberate on the potential applications of the hydrogen energy storage (HES) system for the electric grid and transportation services [13]. Participants emphasized that HES cannot be competitive

with other grid energy storage systems if it is only storing the grid electricity and later converting it back to grid electricity. However, unlike the other grid energy storage system mentioned previously, the HES system is more flexible and can be consumed in more than one way. Other than converting hydrogen back to grid electricity, hydrogen can also be used in the heating and transportation sector which distinguishes a HES system from batteries, pumped hydro, and CAES systems [13].

Due to the specific geographic requirements and the scale of pumped hydroelectric and CAES energy storage, the deployment of such systems are most likely not appropriate for most DOD installations. The choice here then comes to the battery energy storage system or the hydrogen energy storage system. Battery energy storage has been commercialized and has been deployed widely in electric grid applications. Therefore, further study of the integration of battery technology with renewable energy does not yield much benefit to the DOD when industry has already demonstrated and deployed such systems. In order to diversify DOD's energy storage portfolio, this thesis addresses the feasibility of integrating hydrogen energy storage with solar power.

C. PREVIOUS SETUP

For his master's thesis, LT Angel Aviles set up and demonstrated the possibility of producing water, hydrogen, and power using PV cells and ambient moisture [14]. Figure 3 shows the concept design of LT Aviles' system.

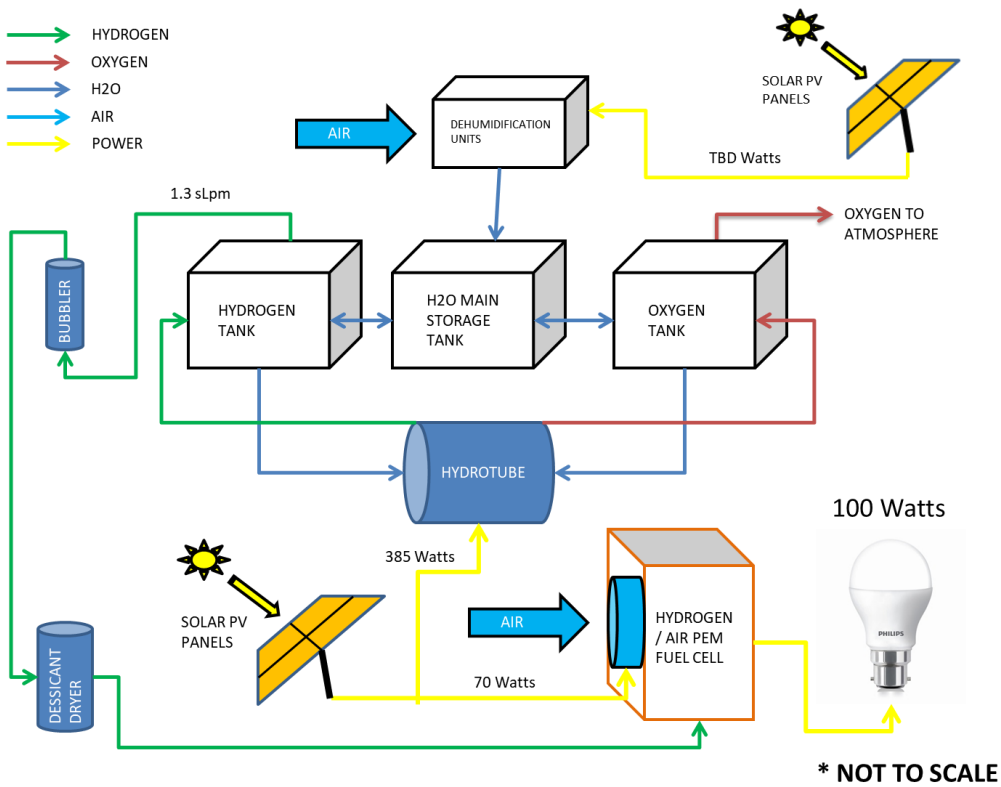

Figure 3. Previous Concept Design Diagram. Source: [14].

1. Electrical System

All components of the system operated with 11 to 13 V electric power and were powered with solar power. Six solar panels were installed in a parallel configuration to power the system. Each panel is rated for 31 V and 8.7 Amp at maximum power. They were connected to a combiner box for a combined maximum output of 1,620 W at 31 V_{mp} and 52.2 Amp_{mp}. The theoretical power requirement of the system was 741.5 W and the solar panels were sized with a safety factor of more than 2 to compensate for fluctuation in output due to weather. In order to supply electric power from the PV cells at 31 V to the system at 11 to 13 V, a MidNite Solar charge controller converted the output PV voltage to the desired system voltage. From the charge controller, power was then routed to an electrical panel to distribute power to each component of the system.

2. Mechanical System

The mechanical system was all gravity fed and achieved by placing each successive component at a lower elevation. Water was the feedstock to produce hydrogen gas by electrolysis. In LT Aviles' design, distilled water was collected from the ambient air using Peltier dehumidifiers, manufactured by Ivation. Water collected from the dehumidifiers was then drained to the main storage tank by gravity to be used to produce hydrogen gas. An alkaline water electrolysis system, manufactured by Hybrid Hydrotech, was used to produce hydrogen and oxygen gas using distilled water with a 15% potassium hydroxide (KOH) concentration as an electrolyte. The electrolysis system consisted of a hydrogen electrolyte storage tank, an oxygen electrolyte storage tank, current limiting device, and an electrolyzer. The main water storage tank was connected to the hydrogen and oxygen electrolyte storage tank for water replenishment. Two valves controlled the flow of water from the main storage tank to hydrogen and oxygen tanks. The valves were normally closed and only opened to replenish water in the hydrogen and oxygen tanks when the electrolyzer is not in operation. After the initial mix, only distilled water was needed to replenish the system because KOH remained in solution when water disassociated into hydrogen and oxygen gas during electrolysis. The 15% KOH solution in the hydrogen and oxygen storage tank was plumbed to the electrolyzer. The solution flowed into the electrolyzer by gravity because the storage tanks are at a higher elevation than the electrolyzer. When electric power was applied to the electrolyzer, water disassociated into hydrogen and oxygen gas. Because the gases were lighter than water, the hydrogen gas rose to the hydrogen electrolyte storage tank and the oxygen gas rose to the oxygen electrolyte storage tank after they were produced. The oxygen gas vented to the atmosphere while the hydrogen in the hydrogen storage tank was routed to the polymer electrolyte membrane (PEM) fuel cell, manufactured by Horizon Fuel Cell Technologies to produce 100 W electric power. To ensure high quality hydrogen gas, the hydrogen gas first passed through a hydrogen bubbler to cleanse any containment. After the hydrogen gas bubbled through the bubbler, it then went through a desiccant dryer to remove moisture before being routed it to the PEM fuel cell because the fuel cell required dry hydrogen gas. A diaphragm pump was installed to boost the pressure of hydrogen gas

going into the PEM fuel cell. Table 2 summarizes the main components of the electrical and mechanical system.

The objective of LT Aviles' thesis was to prove that solar power could be used to produce hydrogen gas from ambient air and then use the hydrogen gas to produce electric power. The object of his thesis was met because the system produced hydrogen gas from ambient air and then used the hydrogen gas, through a PEM fuel cell, to produce electricity to power a 100 W lightbulb. However, the PEM fuel cell could not sustain a steady power generation as LT Aviles pointed out in his thesis [14]. The objective of this thesis was to implement an automated data collection system to better measure and characterize the performance of each component and improve system performance. A secondary objective was to sustain a more continuous hydrogen production and electric power with the hydrogen fuel cell.

Table 2. Main Components of LT Aviles' System

Main Component	**Manufacture**	**Function**
Charge controller	MidNite Solar	Controls output voltage to system
Dehumidifier	Ivation	Produce water
Electrolysis system	Hybrid Hydrotech	Produce hydrogen gas
Diaphragm pump	Ingersoll-Rand	Boost hydrogen gas pressure
PEM fuel cell	Horizon Fuel Cell Technologies	Produce electric power

II. ENABLING TECHNOLOGY

Three enabling technologies enable this system to work as follows: dehumidification, electrolysis, and electrochemical fuel cell.

A. DEHUMIDIFICATION

Ambient air contains a small amount of moisture. According to Dalton's law, the total atmosphere pressure is the sum of the dry air partial pressure and the partial vapor pressure [15]. At any particular temperature, there is a unique saturated vapor pressure for the water vapor. If the partial vapor pressure is greater than the saturated vapor pressure, vapor will compress or condense into liquid. In unsaturated ambient air, the partial vapor pressure is always less than the saturated vapor pressure. However, saturated vapor pressure changes proportionally with temperature. When ambient air is cooled at a constant pressure, the partial vapor pressure remains constant while the saturated vapor pressure decreases. Once the ambient air is cooled to a temperature where the partial vapor pressure and the saturated vapor pressure are the same, the ambient air is saturated, and the temperature is called the dew point temperature. Cooling below the dew point temperature will result in condensation because the partial vapor pressure is greater than the saturated vapor pressure. Therefore, the moisture in the ambient air can be extracted or condensed by cooling it below the dew point temperature and the process is called dehumidification. Dehumidification works by passing ambient air through a coil or fins that are cooler than the dew point temperature.

Sensible heat needs to be removed from the ambient air to lower the temperature to the dew point temperature, and latent heat of vaporization needs to be removed before water will condense. The heat can be removed using a refrigeration cycle or a solid-state system that utilizes the Peltier effect. For this thesis, a dehumidifier uses the Peltier effect was chosen because it is small and lightweight, has no moving parts, and contains no hazardous material. The Peltier effect is produced when electric current flows through a P-type and N-type semiconductor that are connected to each other with two conductors as shown in Figure 4. The heat being transferred from one conductor to another is based on

the direction of the current and the amount of heat transferred matches the electric power consumed [16]. Fins are attached to the cooled side of the conductor in the dehumidifier to enhance heat transfer with ambient air and condense the moisture. However, the power consumed by a Peltier device is fixed at a given voltage and current and so is the heat transferred. The heat must be removed from ambient air before condensation can take place and changes depend on the relative humidity. Therefore, the amount of moisture removed from the air can vary for the same amount of input power.

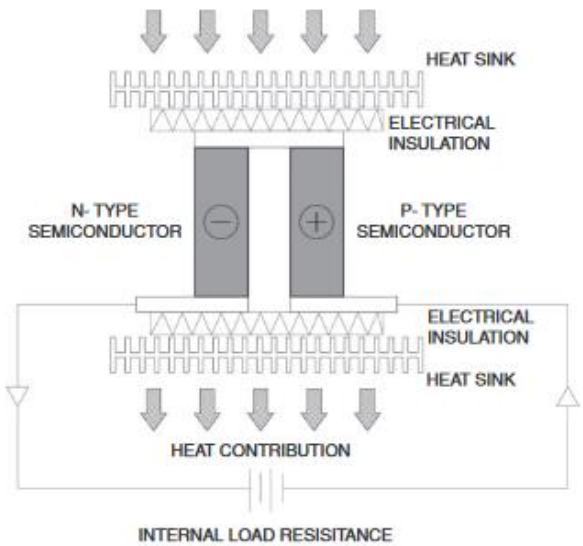

Figure 4. Peltier Effect. Source: [16].

B. ELECTROLYSIS

Electrolysis is the process of disassociating water molecules into hydrogen and oxygen gas by passing an electric current through an electrolytic cell. The basic components of an electrolytic cell consist of an anode, cathode, diaphragm membrane, electrolyte, and a direct current (DC) power supply [17]. Figure 5 shows the basic scheme of an alkaline water electrolysis system. At the cathode, hydrogen ions (H^+) consume the electrons provided by the DC power supply and form hydrogen gas. To satisfy Kirchhoff's current law, the leftover hydroxide ions (OH^-) must transfer through the electrolyte to the anode and give away the electrons to return to the positive terminal of the power supply to complete the circuit. There is a diaphragm membrane in between the

two electrodes. The purpose of the membrane is to prevent the electrodes from touching each other to create a short. Its other function is to stop the recombination of oxygen and hydrogen and selectively allow hydroxide ions to pass through. By giving away the electrons, the hydroxide ions oxidize to oxygen gas and water. The half-cell reactions at the cathode and anode, as well as the overall reaction in an alkaline solution is given by Equation 1, 2, and 3, respectively [16]:

Cathode $$2H_2O + 2e^- \rightarrow H_2 + 2OH^- \quad (1)$$

Anode $$2OH^- - 2e^- \rightarrow 1/2\,O_2 + H_2O \quad (2)$$

Overall $$H_2O \rightarrow H_2 + \tfrac{1}{2}O_2 \quad (3)$$

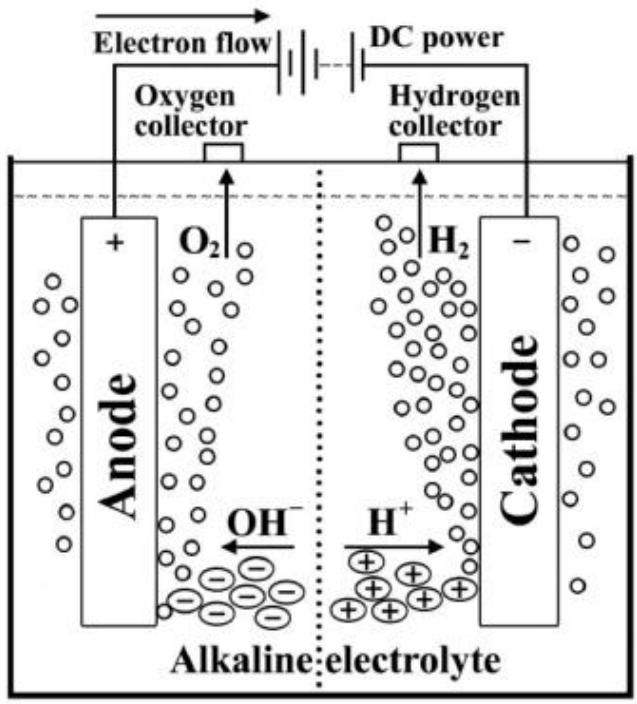

Figure 5. Basic Scheme of an Alkaline Water Electrolyzer. Source: [17].

The total energy required to disassociate water is the change of enthalpy for the reaction shown in Equation 3. Enthalpy is defined by Equation 4, where ΔG is the change

of Gibbs free energy and TΔS is the entropic contribution or loss depending on whether the reaction is non-spontaneous or spontaneous. ΔG is the energy that can do useful work. For electrolysis, ΔG is the electrical energy required. For non-spontaneous reactions like electrolysis, not all energy required is from electrical energy and some the energy is from entropic contribution, which is heat energy. In the case of electrolysis, heat is absorbed from the surrounding electrodes and is replenished when current starts to flow due to resistive loss. However, for spontaneous reactions like a fuel cell, heat is an entropic loss because it is lost and cannot be used for electrical work. Because enthalpy (ΔH) and entropy (ΔS) is approximately constant over the practical temperature range [18], as temperature increases, the entropic contribution increases while ΔG decreases. This is why a high temperature electrolyzer like a solid oxide electrolyzer consumes less electricity than low temperature electrolyzer.

$$\Delta H = \Delta G + T\Delta S \tag{4}$$

In standard temperature and pressure conditions, the value of ΔG is 237.4 kJ mol^{-1}. Based on energy conservation, ΔG must be equal to the amount of electricity required to disassociate water as shown in Equation 5, where n is the number of moles of electrons transferred in the reaction, F is the Faraday constant, and E^0 is the electric potential. Rearrange the equation and the equilibrium electric potential for electrolysis can be calculated as 1.23 V.

$$\Delta G = nFE^0 \tag{5}$$

Thermodynamics equilibrium dictates whether the reaction can happen or not, and electrochemical kinetics dictate at what rate the reaction will take place. Theoretically, at 1.23 V, water will disassociate into oxygen and hydrogen. However, the rate of the reaction is so slow that it has no practical use. According to electrochemical kinetics, overpotentials are needed to increase the reaction rate [19]. Figure 6 shows a typical polarization curve for a low temperature electrolyzer. At low current, the logarithmic voltage increase of the curve indicates the activation energy required for oxygen and hydrogen evolution reaction is more dominant. The activation energy is governed by Nernst equation, which is a logarithmic function. Therefore, as current increases, the activation energy increases slowly to an

asymptote and ohmic resistance of the cell is more dominant. At high current, the overpotentials increase linearly with current. The ohmic resistance of the cell is the cell resistance to ionic transfer. The cell resistance comes from the electrolyte, the diaphragm membrane, and gas bubbles form around the electrodes.

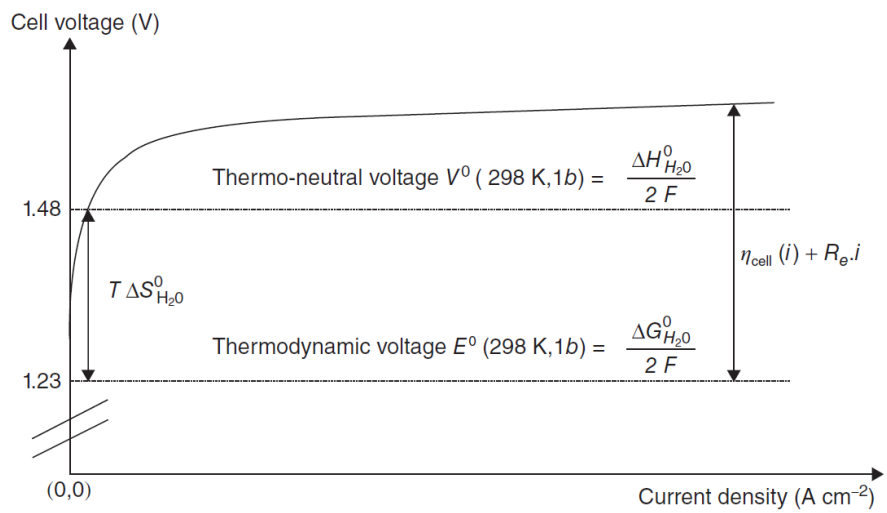

Figure 6. Typical Polarization Curve for Low Temperature Electrolyzer
Source: [18].

Currently, two types of low temperature water electrolysis system – alkaline water and solid polymer electrolyzer are commercially available [18]. The major difference between alkaline water and solid polymer is the electrolyte. The alkaline water electrolyzer, as its name implied, uses alkaline water as the electrolyte. The solid polymer electrolyzer uses a solid polymer called the polymer electrolyte membrane (PEM) as the electrolyte. Because the solid polymer electrolyzer requires the use of an electrode that is embedded with an exotic metal such as platinum and iridium as a catalyst, the cost of a solid polymer electrolyzer is on average eight times more expensive than an alkaline water electrolyzer [14]. Therefore, an alkaline water electrolyzer was used for this thesis.

C. ELECTROCHEMICAL FUEL CELL

An electrochemical fuel cell is a device that converts chemical energy to electrical energy. For a hydrogen fuel cell, hydrogen is the chemical reactant. A hydrogen fuel cell

is basically an electrolyzer in reverse, hydrogen and oxygen are combined to produce electrical energy. The basic operations of a fuel cell are shown in Figure 7. At the anode, the hydrogen gas ionizes and releases electrons. Because the electrolyte is ionically conducting and electrically insulating, the hydrogen ions pass through the electrolyte to the cathode while the electrons pass through the external circuit when a load is connected. On the cathode side, the hydrogen ions recombine with electrons and oxygen to produce water and heat. For every 2 moles of water formed, 4 moles of electrons are produced. Because no combustion occurs in a fuel cell, its efficiency is not limited by Carnot efficiency and can ideally achieve 100% efficiency. However, inherent losses in the electrochemical reaction in a fuel cell reduce fuel cell efficiency.

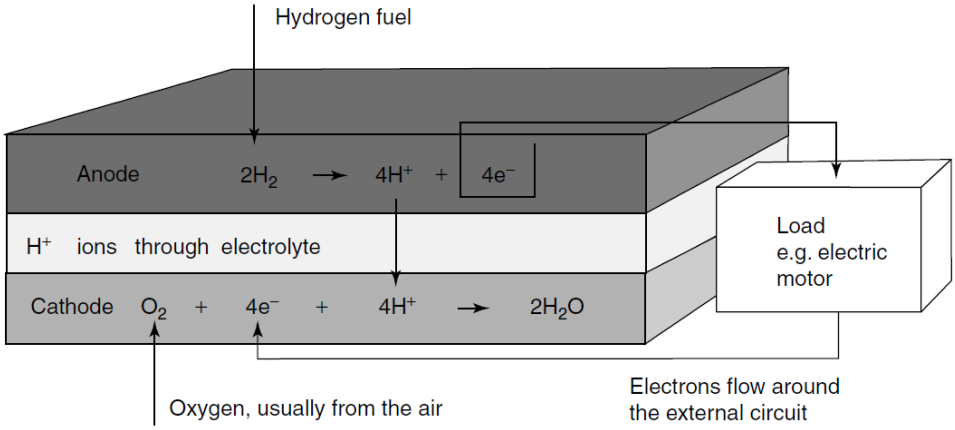

Figure 7. Basic Operations of a Fuel Cell. Source: [20].

Unlike electrolysis, fuel cell reactions are spontaneous and energy is released when water is formed. The total energy is represented by the change of enthalpy of the reaction. However, not all the energy released from this spontaneous reaction can do useful work due to entropic loss. The change of Gibbs free energy (ΔG) is the theoretical useful energy produced when hydrogen and oxygen is combined. ΔG of formation for liquid water in standard temperature and pressure is -237.2 kJ mol^{-1} [20]. Fuel cell converts chemical energy to electrical energy. Based on energy conservation, ΔG released must be equal to the amount of electricity produced. Using Equation 5, the equilibrium electric potential for a low temperature fuel cell reaction can be calculated

and is 1.23 V per cell. The equilibrium potential is also referred to as the no loss voltage [20]. However, due to losses in electrochemical reaction, even at an open circuit, the system voltage is lower than the no loss voltage. The voltage will decrease further when a load is connected to the fuel cell. Figure 8 shows a typical polarization curve for a low temperature fuel cell. Energy from the reaction is lost due to irreversibilities. At low current, the logarithmic voltage drop of the curve indicates the activation loss is more dominant. The activation loss is governed by Nernst equation, which is a logarithmic function, as current increases the activation loss increases slowly to an asymptote and ohmic resistance of the cell is more dominant. Therefore, at high current, the voltage drops linearly with an increase in current. The ohmic resistance of the cell is the cell resistance to ionic transfer and electron flow at the electrodes. The cell resistance comes from the electrolyte.

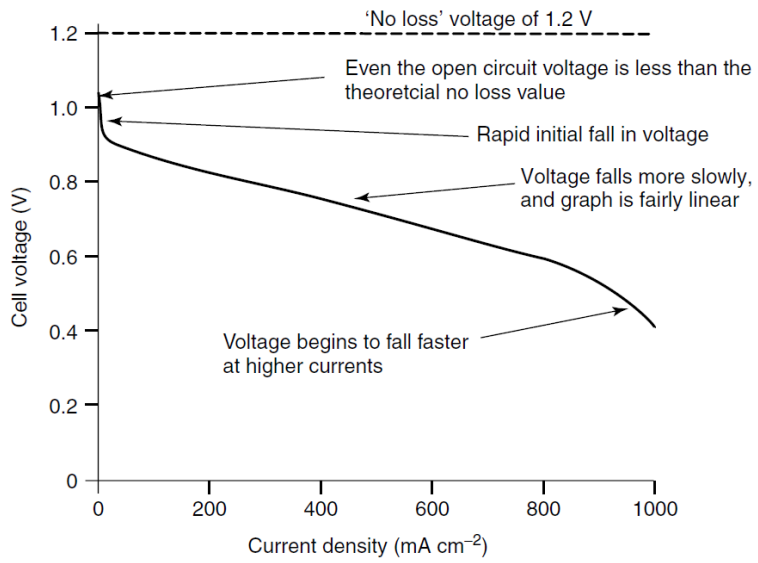

Figure 8. Typical Polarization Curve for Low Temperature Fuel Cell.
Source: [20].

Different types of hydrogen fuel cells have power output ranging from watts to megawatts. However, only the PEM fuel cell has a power output of less than 1 kW. For demonstration purpose, the power output in the kW range for this experiment is not desired. Therefore, a PEM fuel cell was chosen for this thesis.

THIS PAGE INTENTIONALLY LEFT BLANK

III. CURRENT SETUP

A. SYSTEM RECONFIGURATION

1. Electrical

As LT Aviles pointed out in his thesis, the solar panels were installed in a location that were shadowed by a tree line for the greater part of the day and recommended relocating the solar panels for better sun coverage [14]. In order to maximize solar energy production, the solar panels were relocated to the roof of building 216 at the Naval Postgraduate School Turbopropulsion Laboratory. Since more space was available on the roof, three additional solar panels were added to the original array of 6, for a total of 9 panels as shown in Figure 9. The maximum power output increased from 1,620 W to 2,430W. One MidNite Solar charge controller was not rated to handle the additional system power at 12 V, so it was replaced with a Magnum PT100 charge controller that could handle up to 6,660 W at maximum output. The panels were reconfigured to a series parallel configuration as shown in Figure 10. This configuration resulted in a maximum output current of 26.1 Amps and a maximum voltage of 93 V.

The PV array consisted of 3 parallel strings of 3 solar panels in series. Configuring the panels in a parallel configuration like it was previously done was considered. However, because of the new distance between the solar panels and the charge controller was lengthened, the high current generated from a parallel configuration would have required large gauge wire at low voltage (6 AWG vs 00 AWG.) In addition, due to the length of run, voltage drop from the roof to the charge controller was also a concern. Configuring the panels in series was considered as well. However, the maximum operating voltage to the charge controller is 187 VDC. By connecting all the panels in series, this would produce a maximum voltage of 279 V, which was too high for the charge controller.

Figure 9. Picture of Solar Panels on the Roof

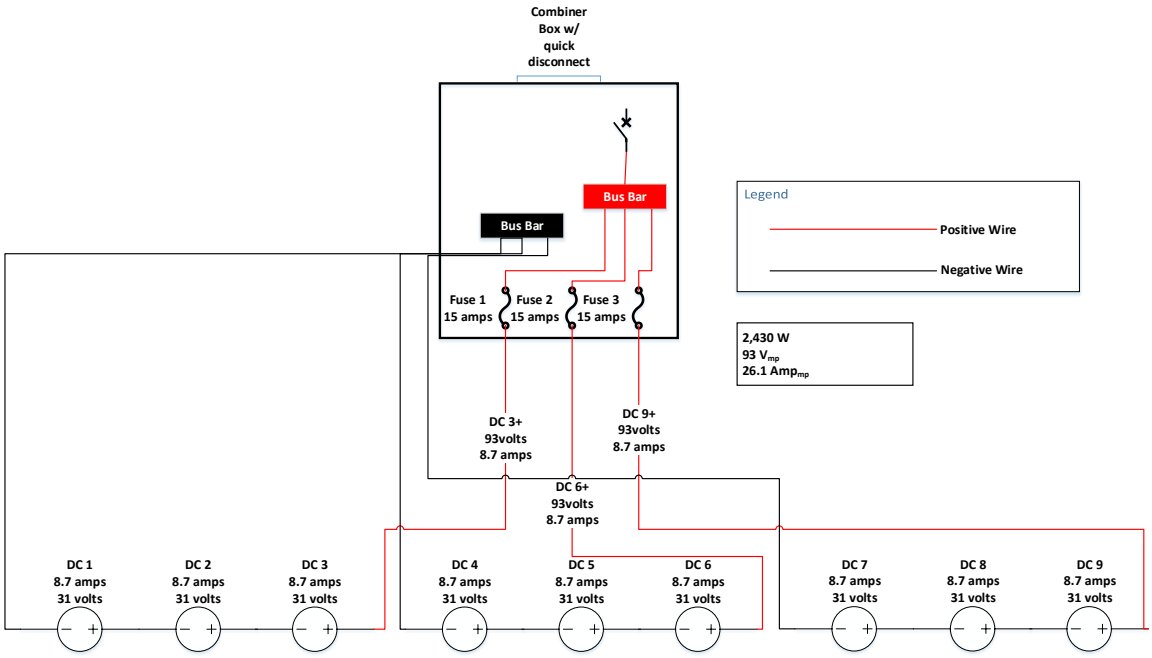

Figure 10. Solar Panel Reconfiguration

Relocating the PV panels to the roof triggered a new NFPA code requirement that all solar panels installed on roof must be equipped with a rapid shutdown [21]. The old combiner box was replaced with a new combiner box which was equipped with a quick

disconnect manufactured by MidNite Solar (MNPV6HV-DISCO 4X). The combiner box with disconnect was relocated to within the array boundary. From the combiner box, the PV wires connected through another quick disconnect at the ground level before connecting to the charge controller at the load. An inverter was not required because all the components of the system operate with direct current (DC) power. From the charge controller, power was distributed to each component of the system via an electrical panel previously set up.

2. Mechanical/Plumbing

Due to safety concern, the system was previously setup in two different locations. The electrolysis system was setup outside in a plastic shed while the dehumidifiers and the fuel cell were setup inside the building as shown in Figure 11. However, to facilitate the operations of the system and minimize hydrogen exposure to the building, the entire system needed to be consolidated and placed outside. A garage style metal shed was constructed to house the entire system as shown in Figure 12. The shed has a 3.658 m x 3.048 m (12 ft x 10 ft) floor space, which was enough space for the entire system and room for expansion in the future to increase hydrogen production. The floor of the shed was lined with anodized aluminum diamond plate so the entire shed was a metal enclosure. A metal enclosure is preferred because of its non-flammability and fire hazard is a big safety concern for hydrogen production and storage.

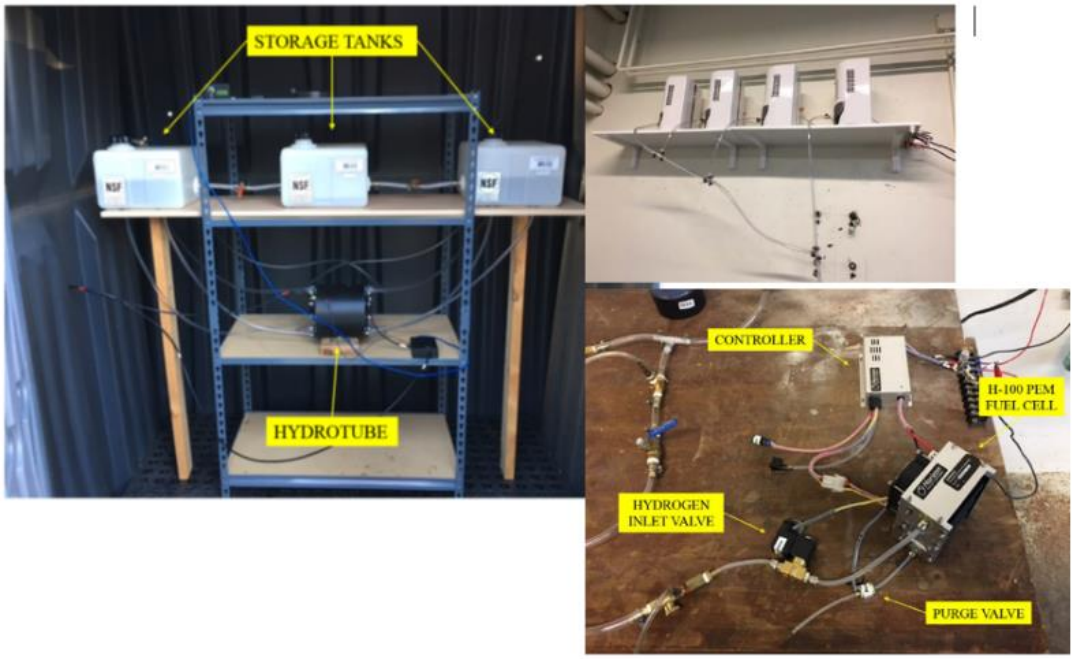

Figure 11. Picture of the System Before Consolidation

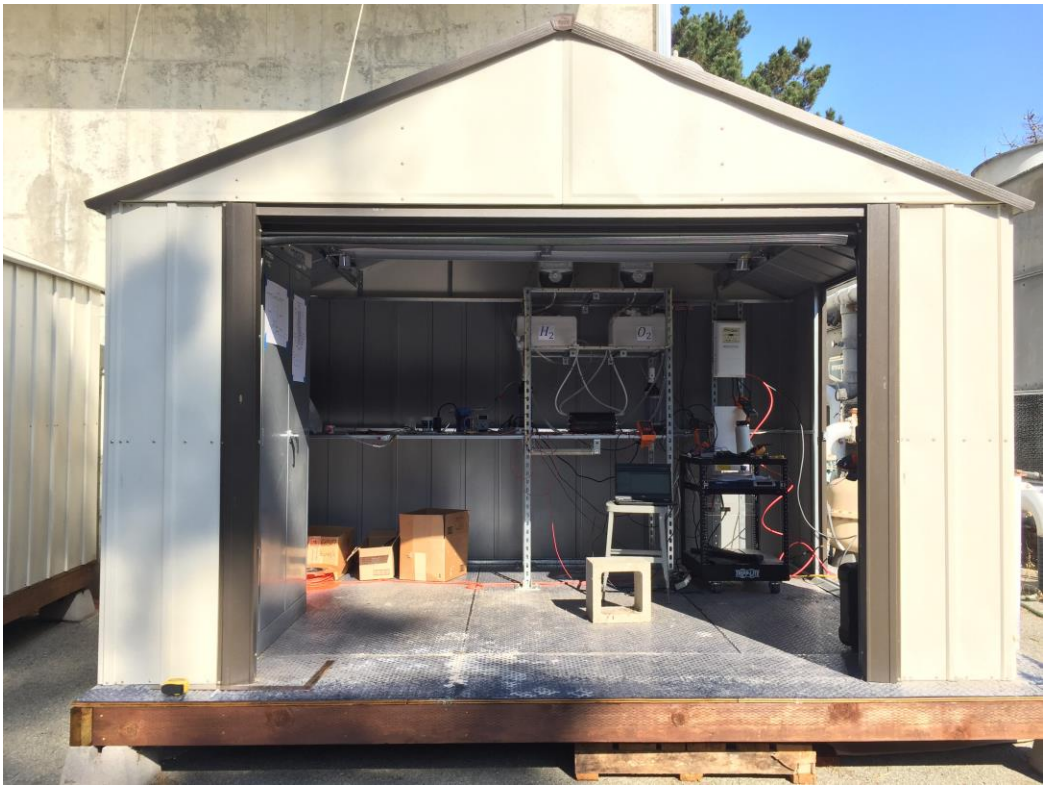

Figure 12. Shed Housing the Hydrogen Production Facility

Once the metal shed was in place, strut channel shelfing was constructed to mount the electrical distribution panel and accommodate each component of the system. Strut channels were used instead of purchasing a prefabricated bench and shelf because they offer more flexibility for expansion. Figure 13 shows the shelfing along with the entire system.

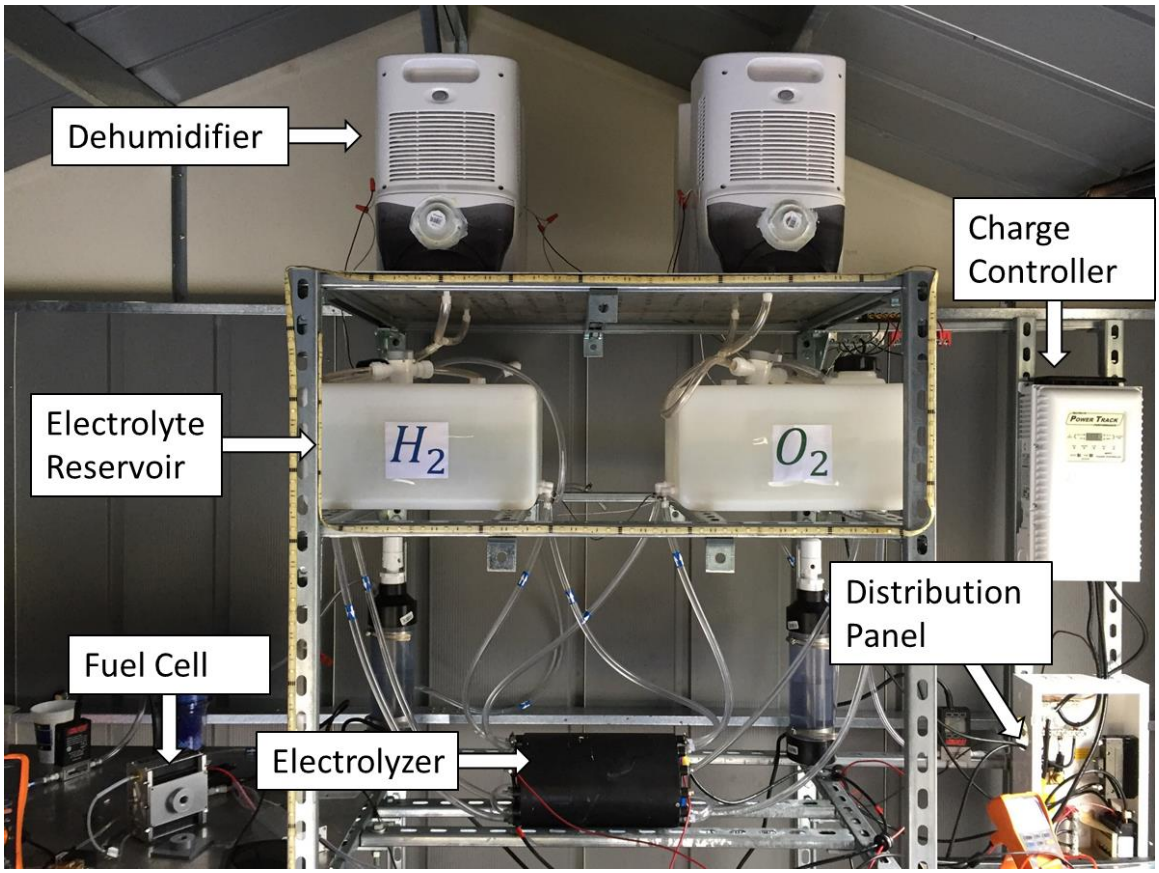

Figure 13. Reconfigured Hydrogen Production Facility

Because the system was designed for gravity fed, 3 levels of shelfing were made. The dehumidifiers were setup on the top level. Previously, the tap was made on the mid level of the reservoir as shown in Figure 14 and water would not start to flow down until the reservoir is half full. A new 6.35 mm (¼”) national pipe thread (NPT) thread to bard fitting was used to tap the bottom of each dehumidifier so that water drained from the bottom of the dehumidifier’s reservoir instead of from the midlevel of the reservoir.

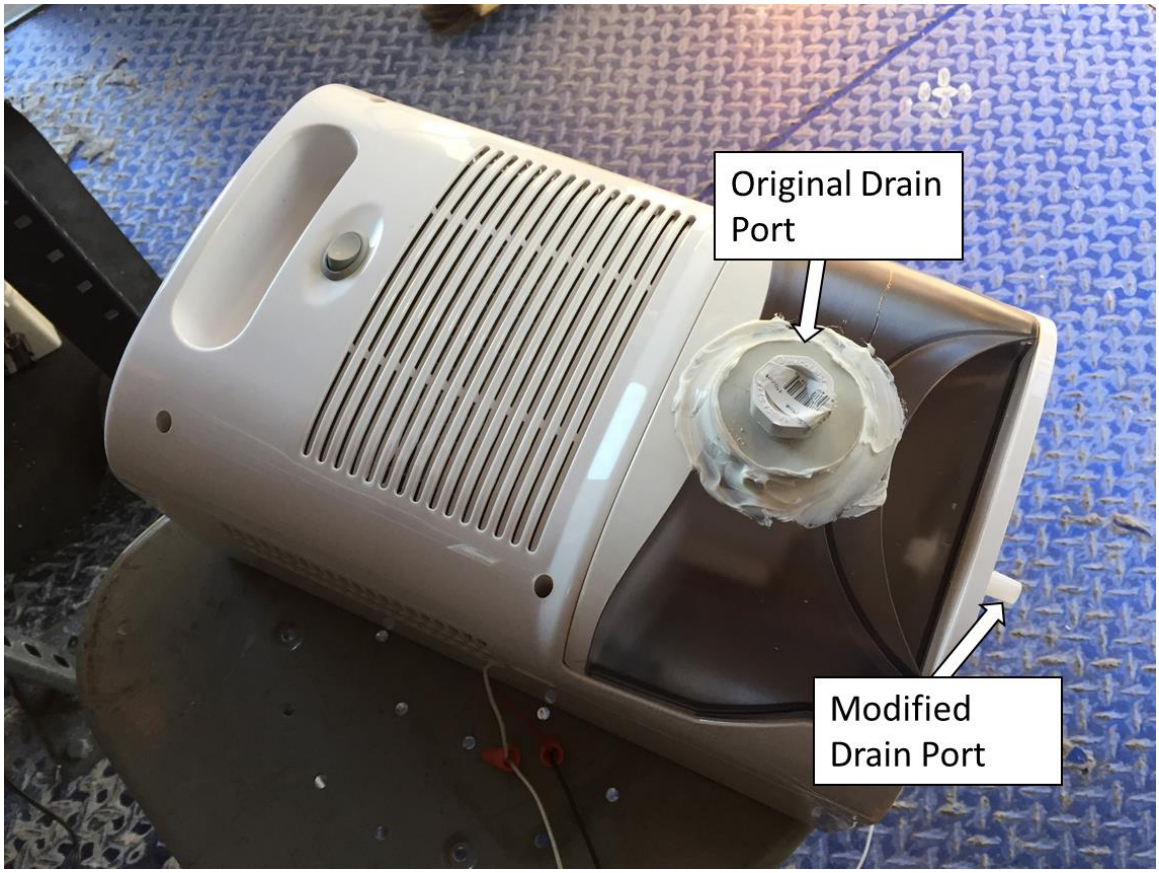

Figure 14. Picture of Modified Dehumidifier Drain Port

The electrolyte tanks were placed on the mid level of the shelf. The main storage tank that was setup previously was removed. There are several reasons for the removal of the main storage tank. First, the electrolyte level on the tanks must be lower than the water entry point, previously at midlevel of the tanks, before replenishment could be made to avoid contaminating the distilled water in the main water storage tank. Secondly, the water level in the main storage tank must be higher than the water exit point before water could flow into the electrolyte thanks. That meant there was always water in the storage tank that could not be used. For these two reasons, the main water storage tank must be positioned above the electrolyte tanks for full utilization. However, each of the dehumidifiers that were above the electrolyte tanks already had a water storage tank. To reduce redundancy, instead of moving the main water storage tank above the electrolyte tanks, the main water storage tank was eliminated. The only downside with using the

dehumidifier reservoirs as water storage tanks was the electrolysis system could not be replenished while running. Because the dehumidifier reservoir was exposed to the atmosphere, by opening the valve to replenish the system, hydrogen and oxygen gas would escape through the reservoir, and system pressure would be lost. Lastly, the electrolyzer was setup on the lowest level of the shelf. Figure 15 shows the plumbing schematic of the redesigned electrolysis system.

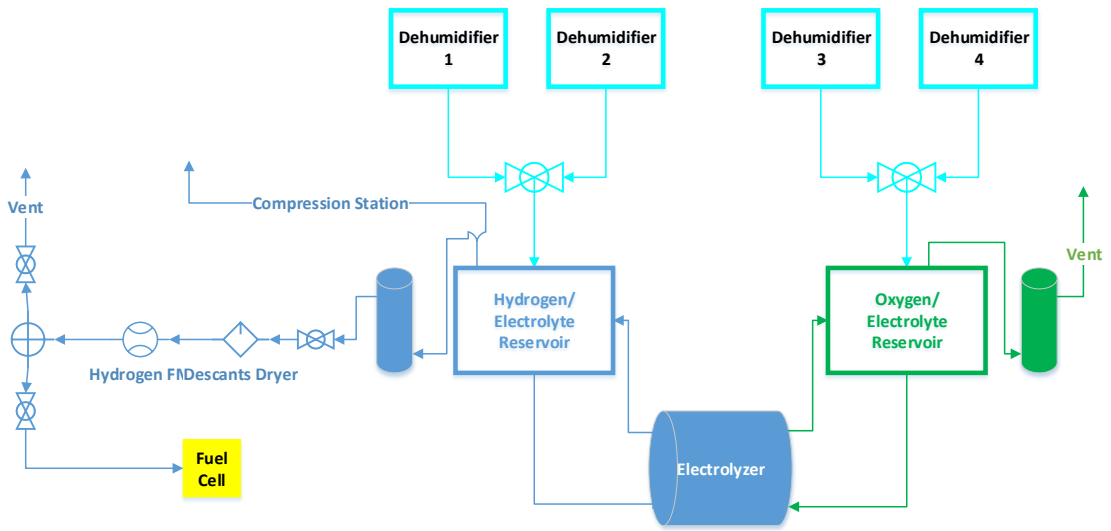

Figure 15. Plumbing One Line for Hydrogen Production System

After the electrolysis system was moved to the shed and reconfigured, a startup test was performed to check for system functionality. As the system began to produce hydrogen and oxygen, an unexpected behavior was observed. The electrolyte level on the hydrogen reservoir dropped while the electrolyte level on the oxygen reservoir rose. This was an indication that system was not balanced. If hydrogen gas and oxygen gas were exiting the system at the same rate as they were being produced, the electrolyte level on both tanks would stay the same. The lower electrolyte level in the hydrogen tank compared to oxygen tank indicated the hydrogen gas was not exiting the system at a slower rate and hence resulted in a higher hydrogen tank pressure. Upon inspection, it was noticed that the path for the hydrogen gas had more resistance than the oxygen gas. The oxygen gas was vented directly to the atmosphere through the bubbler while the

hydrogen gas had to go through the bubbler, a desiccant dryer, and a mass flow meter before it was vented to the atmosphere or fuel cell. The water in the bubbler had two functions – one was to cleanse the gas and the other function was to apply resistance to the gas flow to correct any system imbalance. Therefore, more water was added to the oxygen bubbler in an attempt to mimic the resistance of a desiccant dryer, flowmeter, and the extra tubing resistance since the hydrogen gas had a longer pathway. The system was started again and the electrolyte levels were still not balanced. Since only a limited amount of water could be added to the bubbler and flexibility to change resistance to the oxygen gas was needed for future system expansion, a needle valve was added to the oxygen gas line to control the flow of oxygen. According to the stoichiometric reaction of disassociating water shown in Appendix A, 0.4753 standard liter of oxygen was produced for every standard liter of hydrogen. Theoretically, as long the ratio of hydrogen and oxygen mass flow was maintained, the system would be balanced. A flow meter was added to the oxygen gas line along with the needle valve so the flowrate could be monitored and maintained. The electrolysis system was started again once the needle valve and the mass flowmeter were installed. As anticipated, the flowrate of the oxygen gas was not in the right ratio with the hydrogen gas flowrate. Once the needle valve was adjusted, the desired hydrogen and oxygen flow ratio was maintained. As the electrolyzer ran, the internal pressure changed slightly and the needle value needed to be constantly monitored and adjusted to main the right flow ratio. The needle valve was adjusted based on the electrolyte level of the oxygen tank. If the level decreased, the valve was opened slightly to bring the level back and vice versa. By paying close attention to the electrolyte levels and adjusting the needle valve as needed, the electrolysis system continuously produced hydrogen while keeping the system balanced.

B. AUTOMATED DATA COLLECTION METHOD

In order to characterize the performance of the system components, the gas mass flow rate along with voltage and current data were needed. This was accomplished with use of several devices using software to collect data measurements.

1. Equipment

To measure and capture the hydrogen mass flow, the Alicat M-Series mass flow meter was used. It has an accuracy of ± (0.8% of the reading + 0.2% of full scale). The full scale for the meters used was 5 standard liters per minute (SLPM); therefore, the maximum error in the mass flow data was ±0.05 SLPM. All M series mass flow meters were based on accurate measurement of volumetric flow. The meter also measured the temperature and pressure of the gas. By incorporating the temperature, pressure and compressibility factor into the gas model, volumetric flow rate was converted to mass flow rate corrected to a standard condition. The meter references 25 ^{o}C and 101 kPa as the standard condition and the true mass flow rate could be calculated by multiplying the corrected mass flow rate by the gas density at 25 ^{o}C and 101 kPa. However, because hydrogen had very low density, the true mass flow was very small. Therefore, all data and figure presented in this thesis were in standard volumetric flowrate in SLPM.

The meter equipped with a standard 8 pin min-DIN pin-out that output a RS-232 signal. The signal contained the following flow parameters: pressure, temperature, volumetric flow, corrected mass flow, and selected gas. An Alicat multi-drop box was used to stream the RS-232 signal to a USB interface and then to the computer.

The current and voltage data were measured and captured by Keysight handheld digital multimeter (U1242) and clamp meter (U1213A). Both the multimeter and the clamp meter had the capability to output measurement to a computer via an Infrared to USB cable. The handheld digital multimeter can measured a DC voltage from 100 mV to 1,000 V with an accuracy of ±0.09% of reading and a DC current up to 10 A with an accuracy of ±0.3% of reading. The multimeter could only be used to measure the current of the fuel cell because the dehumidifiers and the electrolyzer drew more than 10 A. The clamp meter could measure a DC voltage from 4 V to 1,000 V with an accuracy of ±0.5% and a DC current up to 1,000 A with an accuracy of ±2.0%. Compared with the multimeter, the clamp meter had a significantly lower accuracy. However, the multimeter could not measure current more than 10 A. Therefore, the clamp meter was exclusively used for applications that require a high current measurement where the multimeter could not be used.

2. Software

Both Alicat and Keysight had software that could be used for data storage by a computer. However, the two software packages could not interface with each other. Therefore, in order to measure and store the flow and electrical data in a synchronized fashion, a different software was needed to log all required measurements. Alicat and Keysight used a serial protocol for data transfer. MATLAB's Instrument Control Toolbox had the capability to communicate with and transfer data from the serial devices without having to write intensive code. Thus MATLAB was used to poll the data from the Alicat and Keysight equipment synchronously. Figure 16 shows the components of the data acquisition system. See Appendix B for MATLAB codes used to measure and store the data for each component.

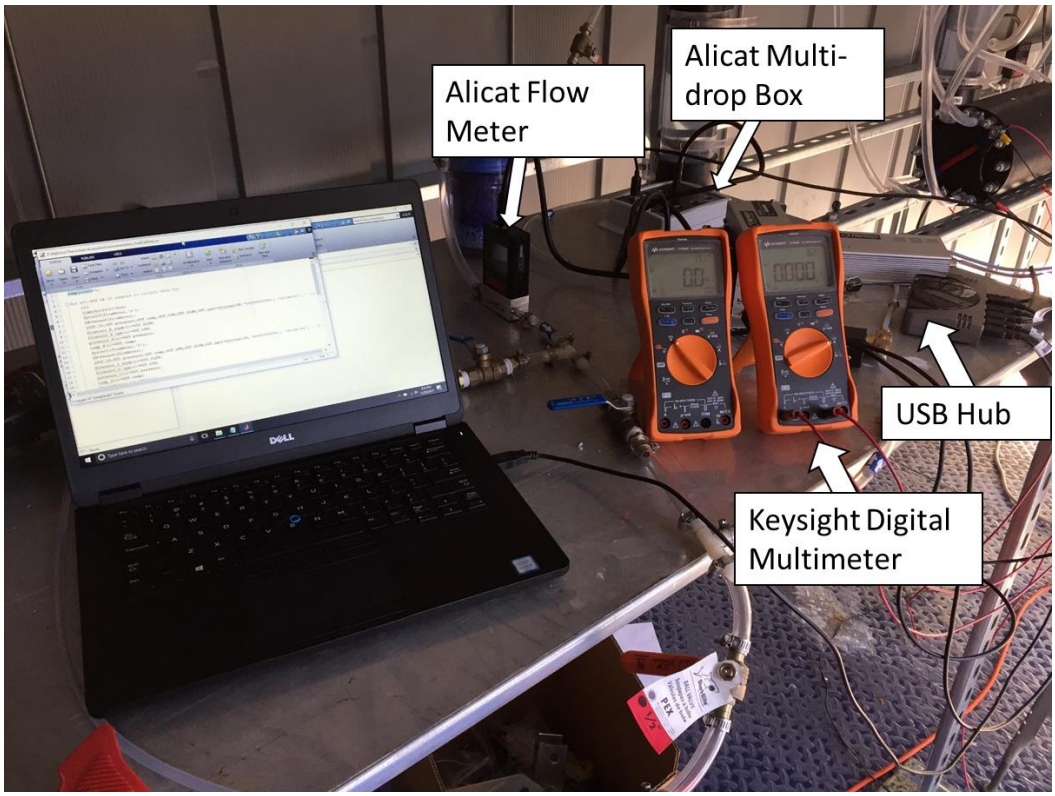

Figure 16. Data Acquisition Components

3. Measurements

Different measurements are needed to characterize the performance of each component. For the dehumidifiers, current, voltage, and the amount of water produced was measured over a 24-hour period. The current and voltage data provided the energy consumption. Using the amount of water produced data, the energy required to produce water was calculated. For the electrolyzer, the hydrogen mass flow rate, current, and voltage data were measured to calculate the power requirement to produce hydrogen at various rates. Hydrogen and electric power were needed to operate the fuel cell which included the supply valve, the exhaust fan, and the controller. Therefore, the current and voltage supplied to the fuel cell were measured and accounted for. The measurements collected during the fuel cell operation are input current and voltage, hydrogen flow rate, and output current and voltage produced by the fuel cell. The hydrogen flow rate along with current and voltage produced by the fuel cell yielded the hydrogen consumption rate for a specific power output. The current and voltage supplied to the system was used as one parameter to calculate system efficiency. Table 3 summarizes measurements taken for each component.

Table 3. Summaries of Measurement Taken

Component	**Measurements Taken**
Dehumidifier	Voltage in, current in, water produced
Electrolyzer	Voltage in, current in, hydrogen mass flow
Fuel cell	Voltage in, current in, voltage out, current out, hydrogen mass flow

THIS PAGE INTENTIONALLY LEFT BLANK

IV. RESULT AND DISCUSSION

A. DEHUMIDIFIER

The amount of water produced by the dehumidifier varies depending on the ambient condition. To gain a general idea of how much water it can produce for a given power input, the dehumidifier was tested on three days with different ambient conditions. The energy consumption of the dehumidifier was measured for a period of 8 hours and Figure 17 shows its energy consumption profile. On average, the current draw was 5.9 Amps at 13 V resulting in a power consumption of 77 W for each humidifier.

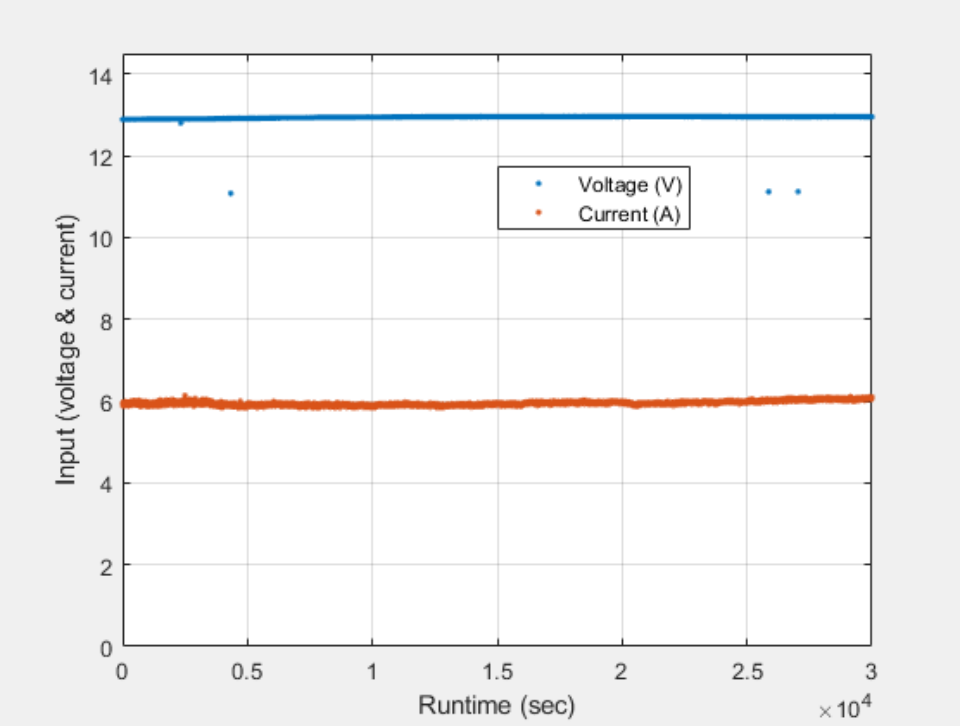

Figure 17. Dehumidifier Energy Consumption Profile

Table 4 shows the results from the three tests along with average dry bulb and dew point temperature data for those days. Using the data collected, the energy consumption was calculated and plotted against the difference between the dry bulb and dew point temperature as shown in Figure 18. As expected, the amount of water produced

varied and depended on the ambient conditions. As the delta between dry bulb and dew point temperature increased, the energy required to produce one gram of water increased. For design purposes, the worst-case scenario was used. Using the worst case scenario, the water production rate for the dehumidifier was 3 g/hr and the energy consumption was 26 Wh/g of water.

Table 4. Water Produced by Dehumidifier on Different Dates

Test date (time)	Runtime (hours)	Water produced (g)	Energy Used (Wh)	Dry bulb/Dew point Temperature (^oC)
21 Oct (0800 to 1827)	10.45	84	805	15.5/7.7
21 Oct (1827) to 22 Oct (0800)	13.55	121	1043	12.4/8
23 Oct (0800 to 1814)	10.23	40	788	25.7/10.1
23 Oct (1814) to 24 Oct (0758)	13.73	55	1057	19.2/6.3
24 Oct (0758 to 1807)	10.15	30	782	27.2/8.5
24 Oct (1807) to 25 Oct (0841)	14.57	75	1122	19.6/6.7

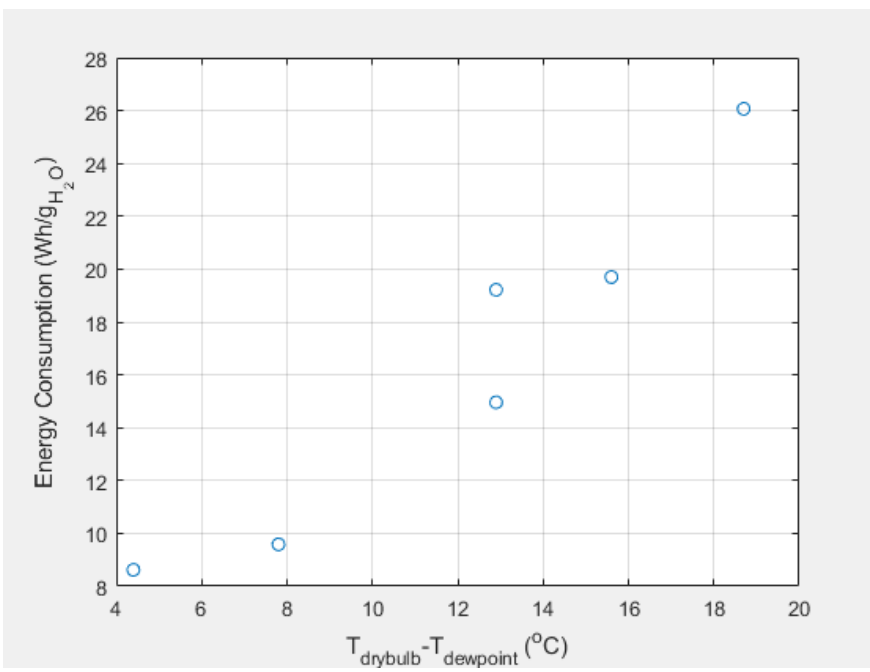

Figure 18. Energy Consumption per Gram of Water vs Temperature Difference ($T_{drybulb} - T_{dewpoint}$)

B. ELECTROLYZER

Using a power supply, the electrolyzer was operated by varying voltages and currents to simulate the intermittent nature of solar power. The first experiment was conducted by varying the voltage supplied to electrolyzer while the second experiment was conducted by varying the current supplied to the electrolyzer. The detailed experimental results were shown in Appendix C. Figure 19 shows the relationship between voltage and current for the electrolyzer. As voltage increased, the current drawn by the electrolyzer increased. The higher voltage increased the chemical reaction within the cell, which must be balanced by the electrons from the external circuit. Similarly, when the current supplied to the electrolyzer decreased, the voltage of the electrolyzer decreased and vice versa. This is important to know because the electrolyzer was the biggest load on the circuit and dictated the circuit voltage. Since the dehumidifiers had an operating voltage of 11 to 13 V, the current supplied to the electrolyzer must be controlled to have a voltage of 11 V to 13 V to avoid damage to the circuitry of the dehumidifiers when the system is automated in the future.

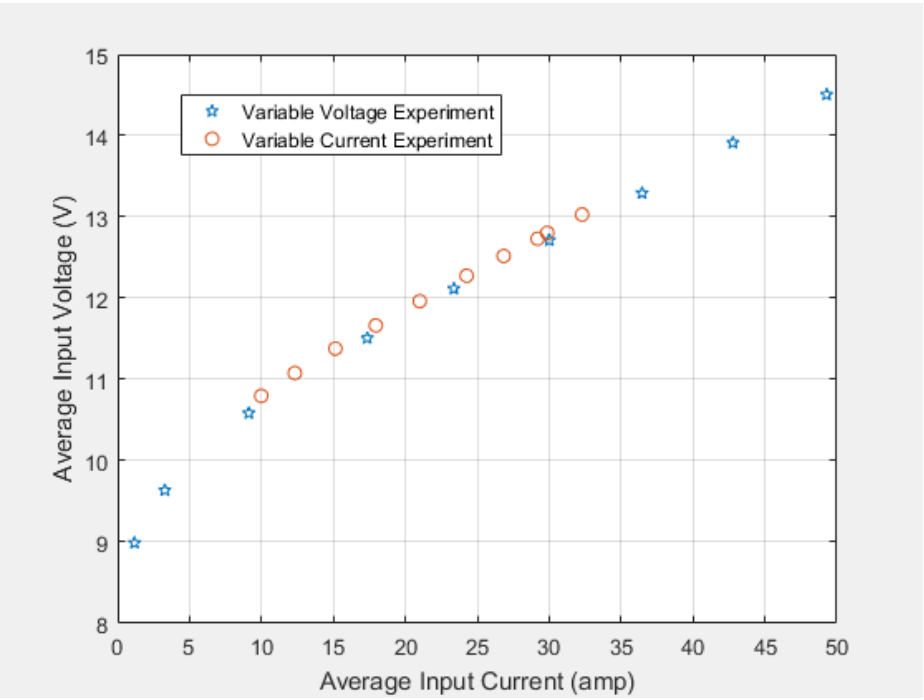

Figure 19. Electrolyzer Current-Voltage Polarization Curve

At low current, the exponential nature of the polarization curve indicated that the activation energy was more dominant. As the current increased, the curve started to become linear and energy required to overcome transport resistance was more dominant.

The electrolyzer demonstrated great flexibility in operating with intermittent power during the experimentation. It produced hydrogen at various voltage and current combinations and did not require a particular voltage and current to produce hydrogen gas as long as the supplied voltage was higher than 9 V. At 9 V, no hydrogen was produced. As the power available increased, the hydrogen production increased and vice versa. Figure 20 shows the relationship between power input and the rate of hydrogen production. Linear regression was used to fit the data and yielded a R-square of 0.99, which indicated that the regression model was adequate. Based on the slope of the regression model, the power required for the electrolyzer was 322 W per SLPM of hydrogen gas.

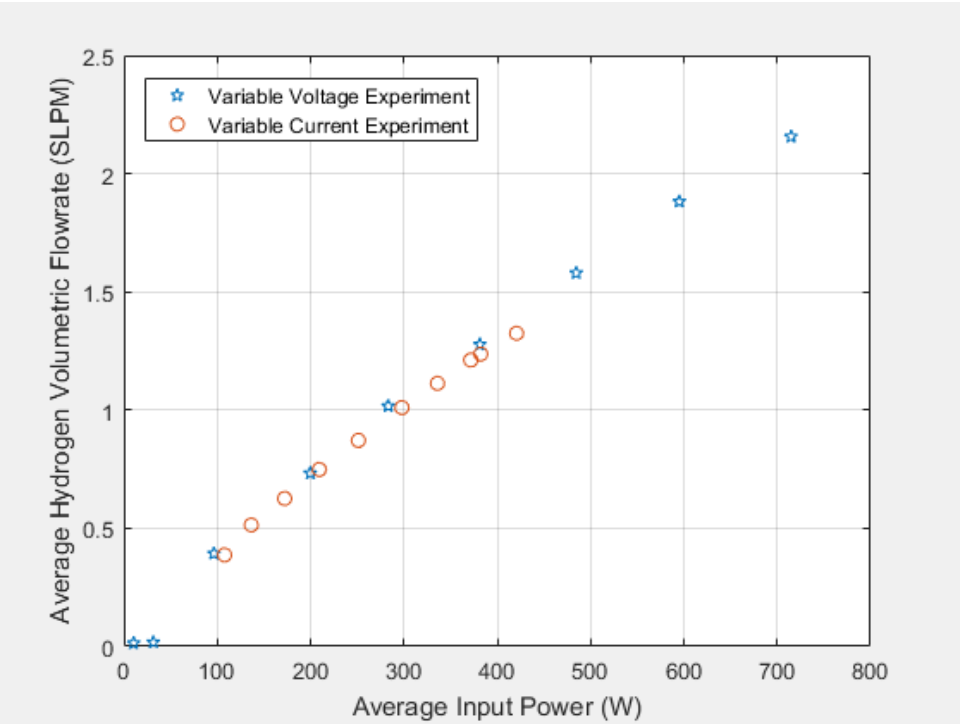

Figure 20. Power and Hydrogen Flowrate Ratio

As the power absorbed by the electrolyzer increased, the hydrogen production rate increased. More power could be supplied to the electrolyzer by increasing the supplied voltage to increase hydrogen production. However, as more power was supplied to the electrolyzer, because of its internal resistance, more heat was generated. The excess heat could damage the gaskets and the membranes that separated the oxygen and hydrogen gas. The manufacture of the electrolyzer recommended an operating voltage of 12 to 14 V. Therefore, operating the electrolyzer at a voltage higher than 14 V could potentially damage internal components and degrade the quality of hydrogen produced. As mentioned previously, operating the electrolyzer at high power also increased the circuit voltage and could damage other components on the circuit connected in parallel with the electrolyzer. However, a standalone stress test could be performed on the electrolyzer by operating it at a higher voltage to test its limit. Before the test is conducted in the future, a hydrogen gas purity analyzer will need to be in place to monitor the quality of hydrogen gas.

Even though the hydrogen production rate increased with input power, because of the excess heat generated with higher input power, both experiments showed that the efficiency of the electrolyzer dropped as the hydrogen production rate increased as shown in Figure 21. Because hydrogen could be combusted in a thermal engine or fed through a fuel cell to extract the stored energy, efficiency could be calculated using either the heating value or the change of Gibbs free energy of water formation. The lower heating value (LHV) of the hydrogen was chosen because Department of Energy (DOE) used LHV to calculate and publish the current electrolyzer efficiency. The calculation from hydrogen flowrate to power using LHV was provided in Appendix A. The efficiency ranged from 63% at low power input to 50% at the highest test power input. This was comparable to water electrolysis efficiency of 67% published by DOE [23].

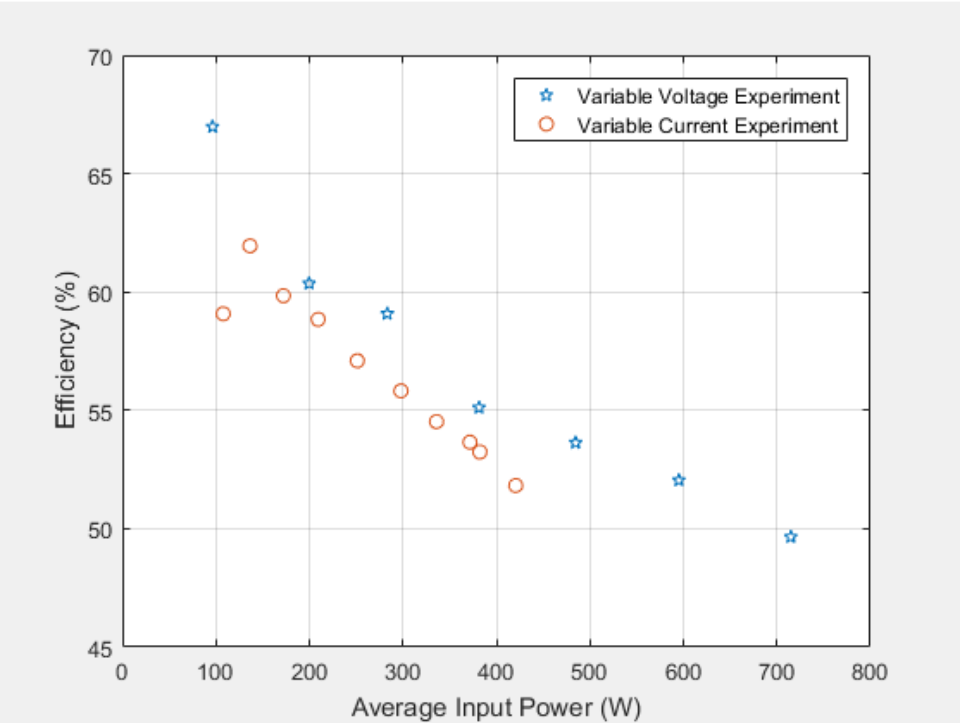

Figure 21. Electrolyzer Efficiency versus Input Power

C. FUEL CELL

To simulate different load conditions, a variable resistor shown in Figure 22 was used. The resistor was connected to the fuel cell circuit and the fuel cell became the power source for the external load. According to Ohm's law, the current flowing through a DC circuit is inversely proportional to the load resistance. Therefore, by changing the circuit resistance, the current will change.

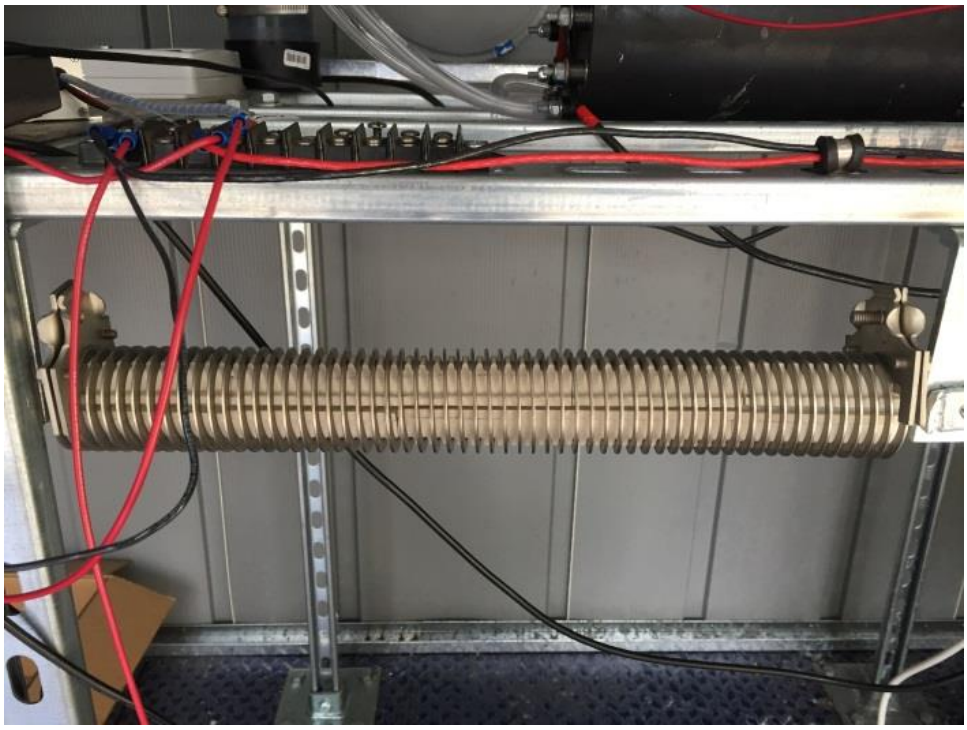

Figure 22. Picture of Variable Resistor Used

Figure 23 shows the current-voltage (IV) polarization curve for the H-100 PEM fuel cell generated using the experimental data. The fuel cell had an open circuit voltage of approximately 19 V. As the current in the circuit increased, the voltage of the fuel cell decreased which is typical for a fuel cell. The initial steep voltage drop was attributed to the activation barrier and is referred to as the activation polarization region [22]. As current increased, linear voltage decreased because of electrolyte resistance to ions; also referred to as the Ohmic polarization region. Figure 24 shows another way to look at it using an equivalent circuit. The fuel cell served as a DC source with some internal resistance. For a typical regulated DC source, as current increased, as long as the internal resistance was kept small, voltage out to the load approximated to the open circuit voltage. However, in the case of a fuel cell, internal losses appeared to be increasing as current increased; therefore, the voltage available to the load decreased. This increase in losses was likely due to the fact that more hydrogen ions had to travel to the cathode and effectively increased the electrolyte resistance. Output power was also included in the

polarization curve. As the current increased, even though the voltage decreased, the power increased.

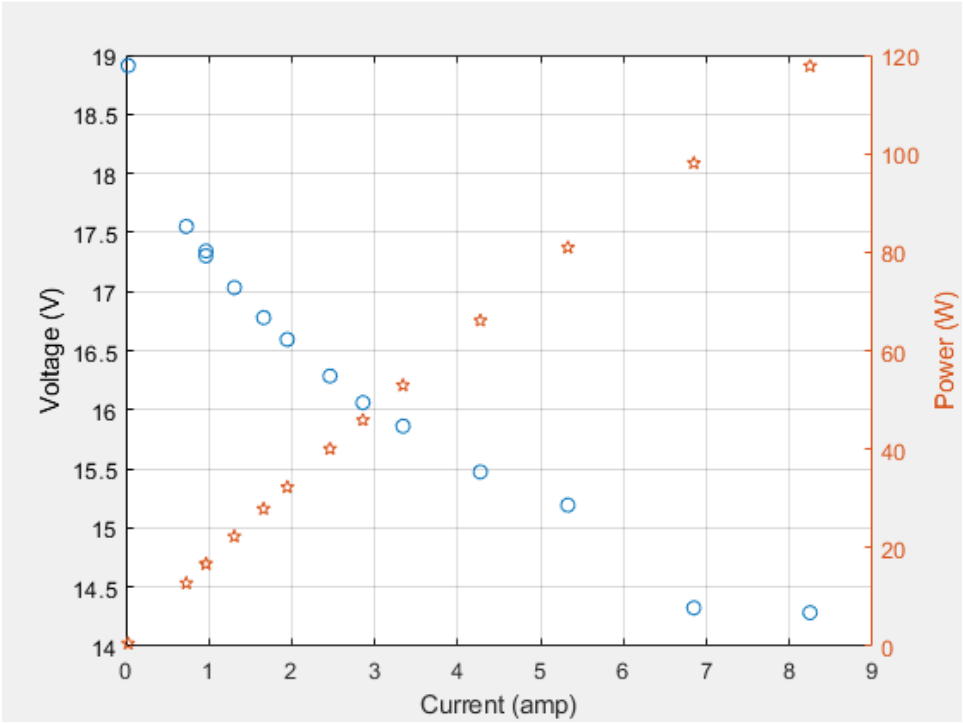

Figure 23. Current-Voltage (IV) Polarization Curve H100 Fuel Cell

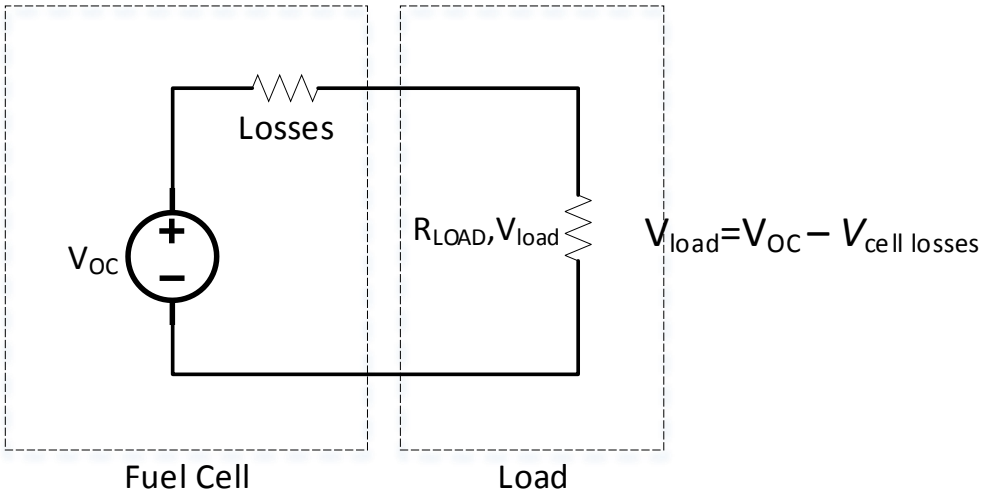

Figure 24. Fuel Cell Load Circuit

Figure 25 shows the relationship between the power output of the fuel cell and the hydrogen volumetric flowrate as well as efficiency. As the flowrate of hydrogen increased, the power output increased as expected. However, efficiency decreased as the power output increased. This was due to the increase in internal losses. More hydrogen ions were needed to travel to the cathode to produce a higher power output. In addition, at a higher hydrogen flowrate, due to the rate of electrochemical reaction at the anode, not all hydrogen atoms were converted to hydrogen ions, which resulted in less hydrogen gas being utilized.

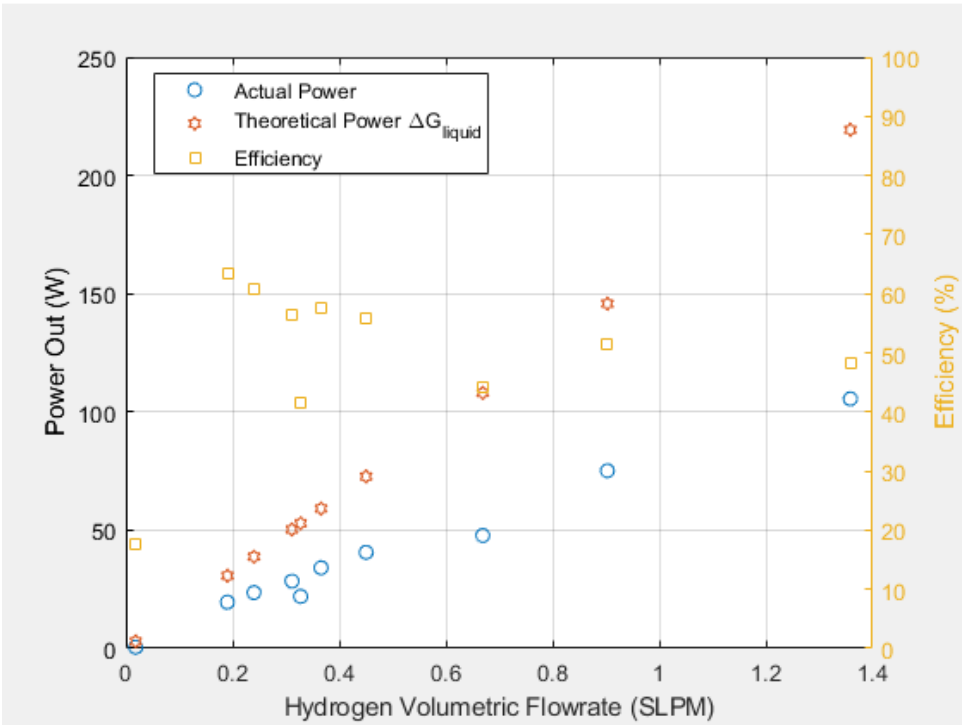

Figure 25. Fuel Cell Efficiency Curve

Another experiment conducted was to inject oxygen produced by the electrolyzer directly into the air intake of the fuel cell. The fuel cell used an exhaust fan for cooling, which pulled in ambient air. The chemical reaction for the fuel cell only required hydrogen and oxygen. Ambient air contains approximately 21% oxygen by volume. Therefore, it was hypothesized that by injecting oxygen produced by the electrolyzer directly into the fuel cell, the fuel cell would perform better. Three dimensional printing

was used to print an adapter that was mounted on the air intake side of the fuel cell as shown in Figure 26. The adapter had a 12.7mm (½") opening, in which the oxygen tube was inserted.

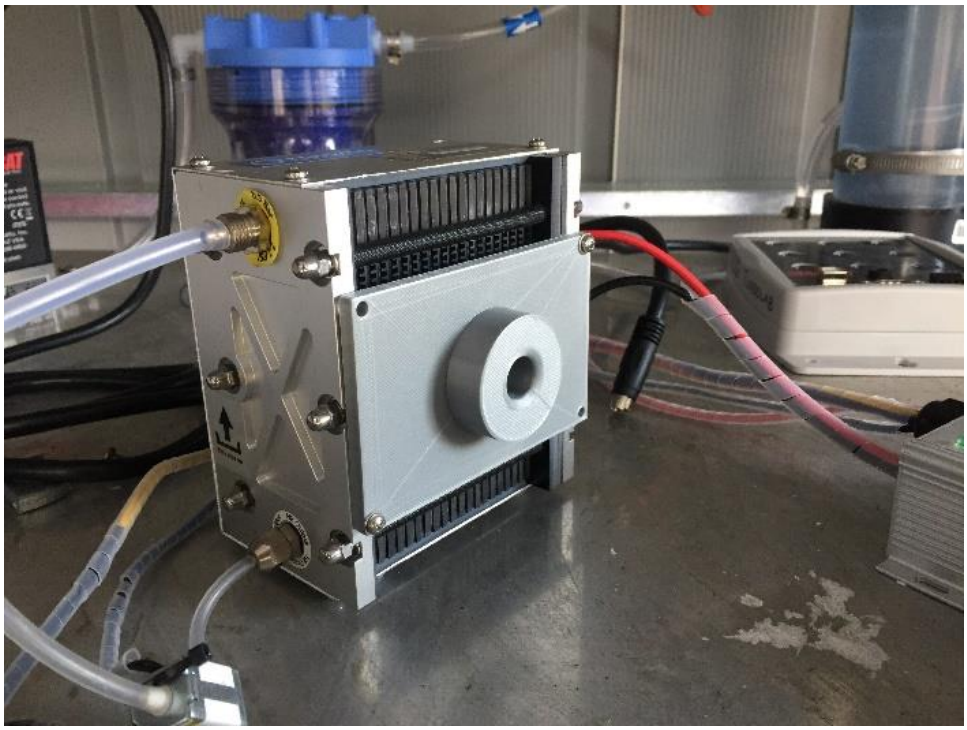

Figure 26. Picture of 3D Printed Oxygen Adapter

The power output and hydrogen volumetric flowrate data from both with and without oxygen injection runs were plotted and compared. From Figure 27, the performance of the fuel cell was slightly better when it was supplied with pure oxygen instead of ambient air. The power output was higher when the fuel cell was supplied with oxygen for any given hydrogen volumetric flow. Because the oxygen intake was not entirely covered with the mount, when the exhaust fan came on, oxygen supplied to the fuel cell was mixed with ambient air. The fuel cell might have performed even better had the intake been completely sealed and supplied with pure oxygen.

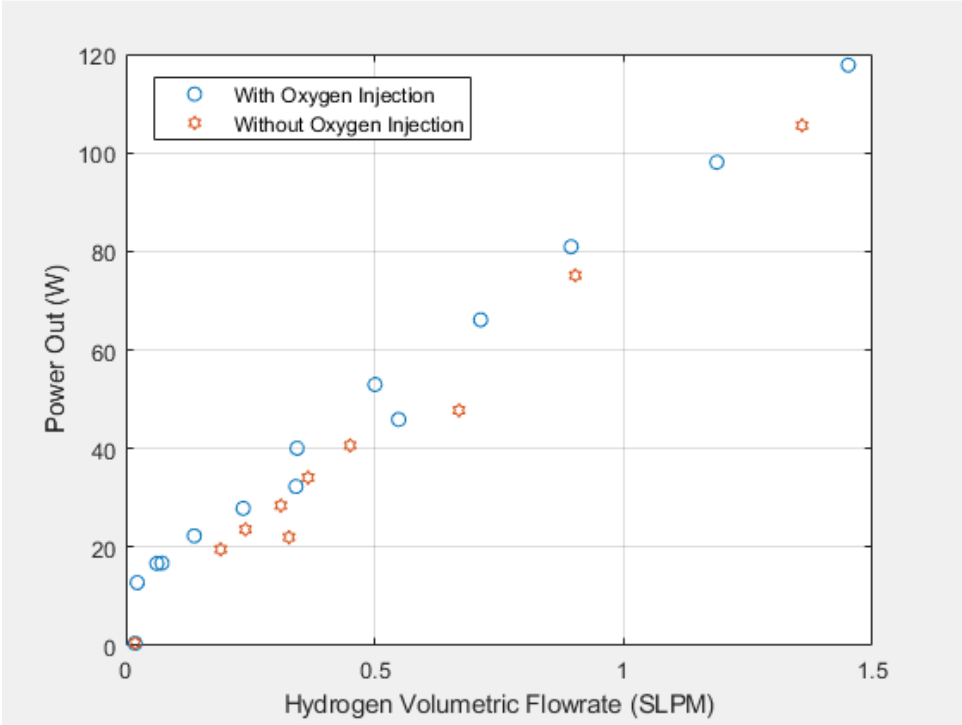

Figure 27. Fuel Cell Performance Comparison—with and without Oxygen Injection

Even though variable resistor nicely simulated different load conditions to generate the IV curve and measure the power output vs hydrogen volumetric flowrate, it became hot quickly once current started flowing through it, and the resistance changed as temperature of the resistor increased. Therefore, it could not be used as a stable load to characterize the fuel cell performance as a function of time. An 100W incandescent light bulb was used to test the performance of the fuel cell as a function of time. The H-100 fuel cell was equipped with an optional short-circuit function to condition the cells every 10 seconds for 100 milliseconds. The manufacturer claimed that by turning the short-circuit function off, the fuel cell performance would degrade by at least 20%. Fortunately for the incandescent light, short-circuiting every 10 seconds was not a problem. But for other loads, like a computer, it might not function well or function at all with a power interruption every 10 seconds without a UPS. Therefore, the fuel cell was tested with and without the short-circuit function on to see how it performed. Figure 28 shows the voltage, current, and hydrogen flow data both with and without the short-circuit function

on. For the first 200 seconds, the short-circuit function was on and for the remainder of the experiment, the short-circuit function was off. When the short-circuit function was turned off, both the voltage and current of the fuel cell decreased as the runtime increased. After more than 2500 seconds later, the performance of the fuel cell continued to degrade and was expected to degrade further.

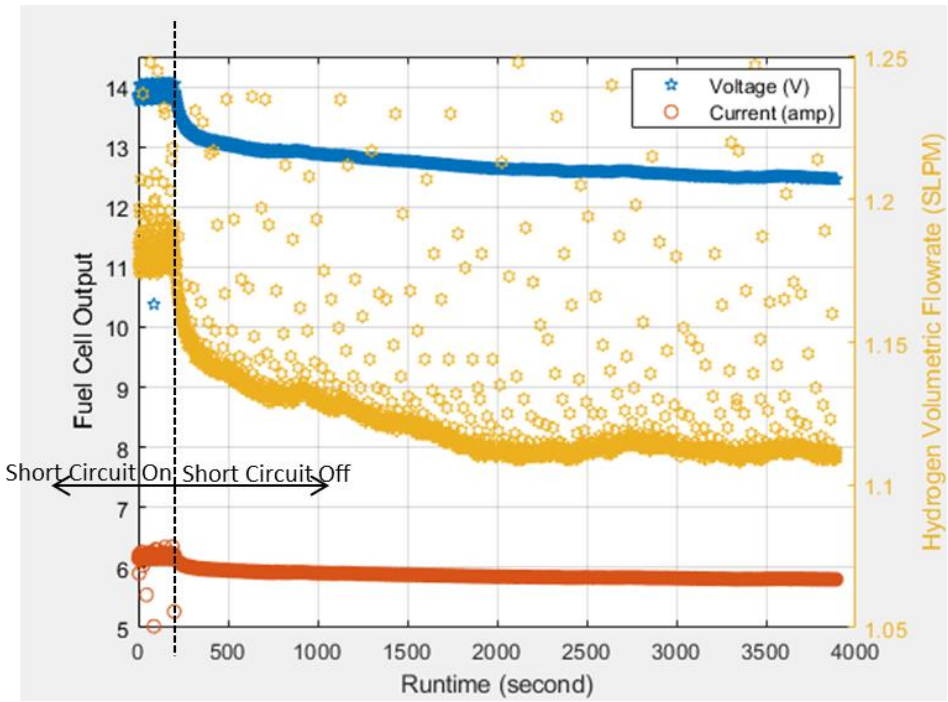

Figure 28. Fuel Cell Performance Characteristics with 100W Lightbulb Load—Overall

Figure 29 shows the data when the short-circuit function was on. On a 10 second cycle, the voltage, current, and hydrogen flow would slowly decrease and go back up. By short-circuiting, the fuel cell restored degraded system performance. It was not clear why the system performance degraded and why short-circuiting was needed. Because dry hydrogen gas was supplied to the fuel cell, one possible explanation was to stop the flow of hydrogen to humidify the membrane and restore performance. A study done by Tribhuvan University demonstrates that the drying effects of reactant gas degraded fuel cell performance [24].

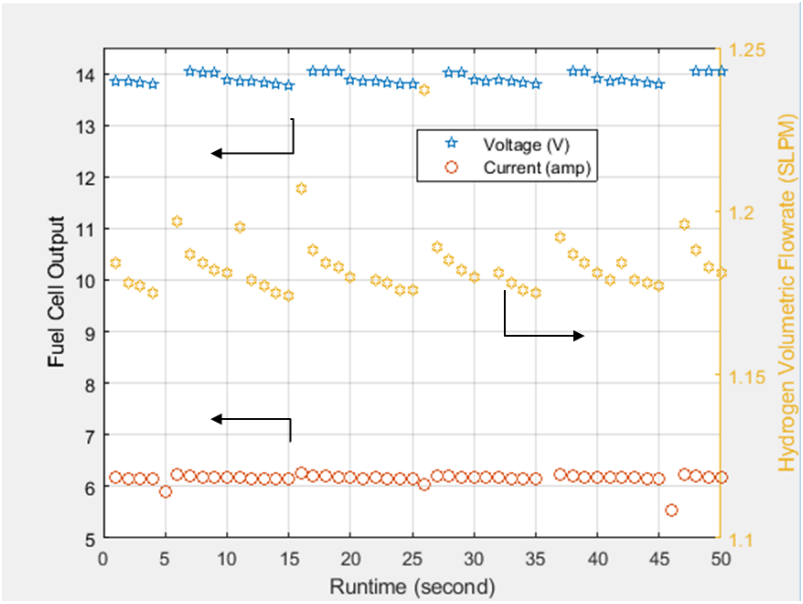

Figure 29. Fuel Cell Performance Characteristics—Short-Circuit On

Figure 30 shows the performance degradation in terms of power when the short-circuit function was turned off. Power loss reached 17% toward the end of the experiment.

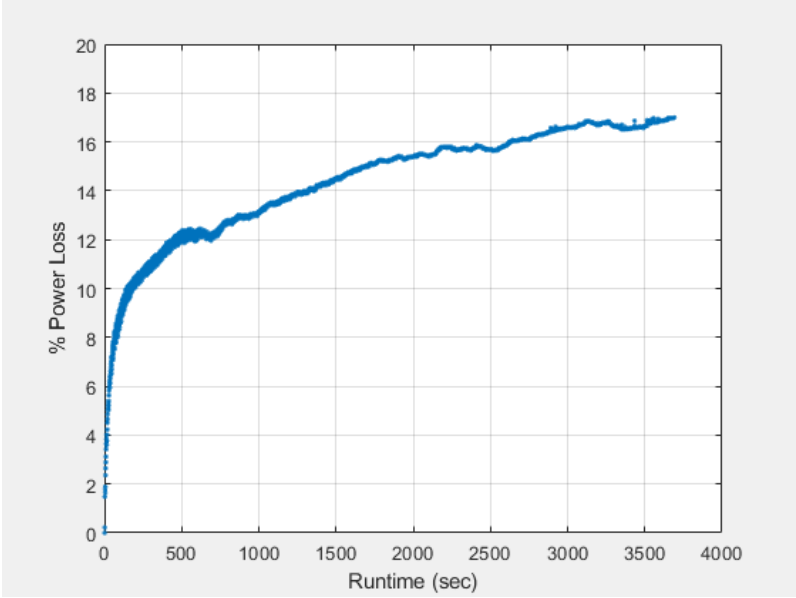

Figure 30. Fuel Cell Performance Loss with Short-Circuit Off

Figures 31 and 32 shows the fuel cell efficiency with and without the short-circuit function. With the short-circuit function on, the fuel cell had an efficiency of about 39% at supply power to the incandescent light bulb. When the short-circuit function was turned off, the fuel cell's efficiency decreased to lower than 32% toward the end of the experiment. This indicated when the fuel cell was not reconditioned every 10 seconds, more hydrogen gas was unreacted and passed as excess fuel.

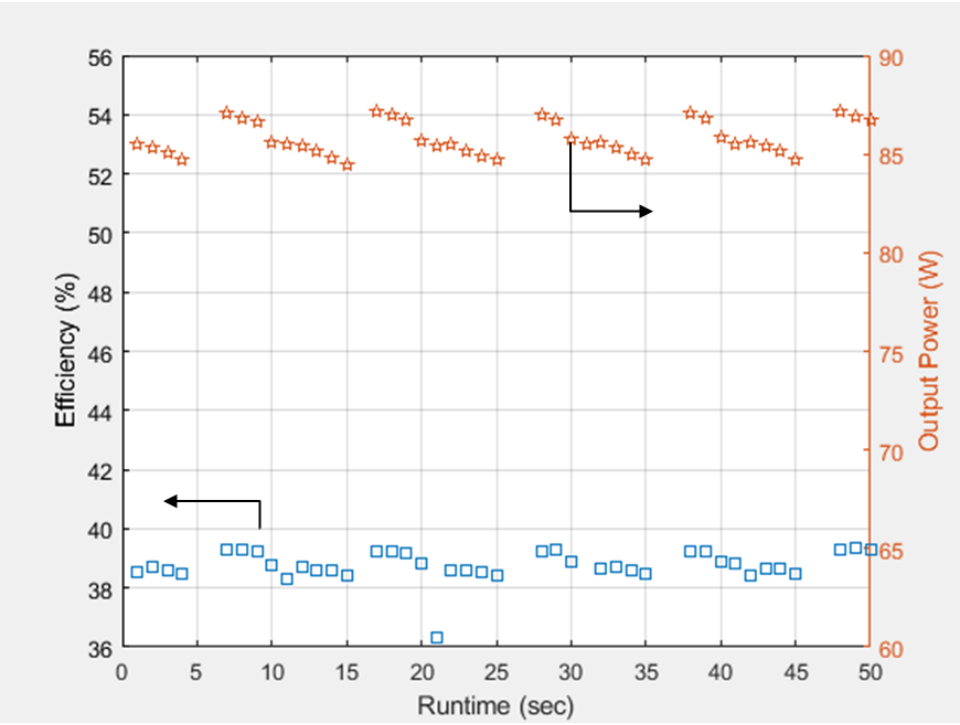

Figure 31. Fuel Cell Efficiency with Short-Circuit On

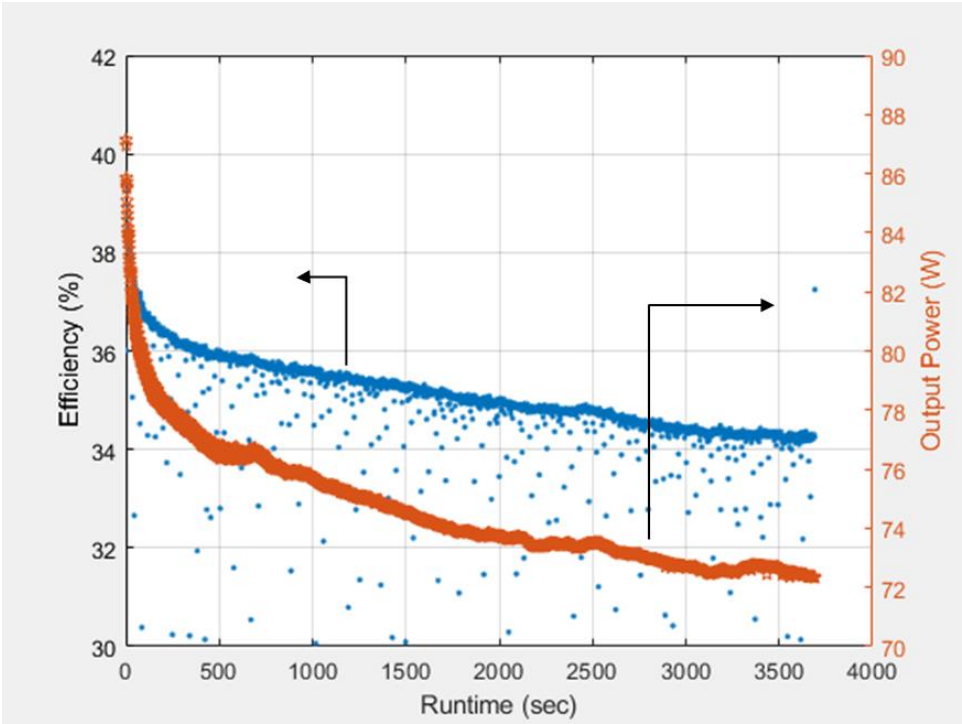

Figure 32. Fuel Cell Efficiency with Short-Circuit Off

D. SYSTEM EFFICIENCY

Using the performance data from the dehumidifier, electrolyzer, and fuel cell, the system efficiency was calculated. System efficiency was examined with two approaches. One approach was to define efficiency in terms of power, and the other approach was to define efficiency in terms of energy. For both approaches, the starting point is to define the output requirement. For the power approach, the output requirement was the desired output power by the fuel cell. Based on the fuel cell output power, the fuel cell power and hydrogen flowrate data (Figure 27) was used to interpolate the hydrogen flow required to produce the desired power. Once the hydrogen flow requirement was known, the electrolyzer power and hydrogen flow data (Figure 20) was then used to interpolate how much power the electrolyzer needed in order to produce the hydrogen flowrate. Using the hydrogen flowrate requirement, the amount of water required was calculated. Based on calculations contained in Appendix A, producing one SLPM of hydrogen required 0.7395 gram/min of water. Using the water production rate of the dehumidifier, the number of dehumidifiers needed was calculated. Multiplying the number of dehumidifiers by the

power consumption of each dehumidifier yielded the power requirement for the dehumidifiers. Figure 33 summarizes the process of how the power requirement for the electrolyzer and dehumidifiers are determined based on fuel cell output power.

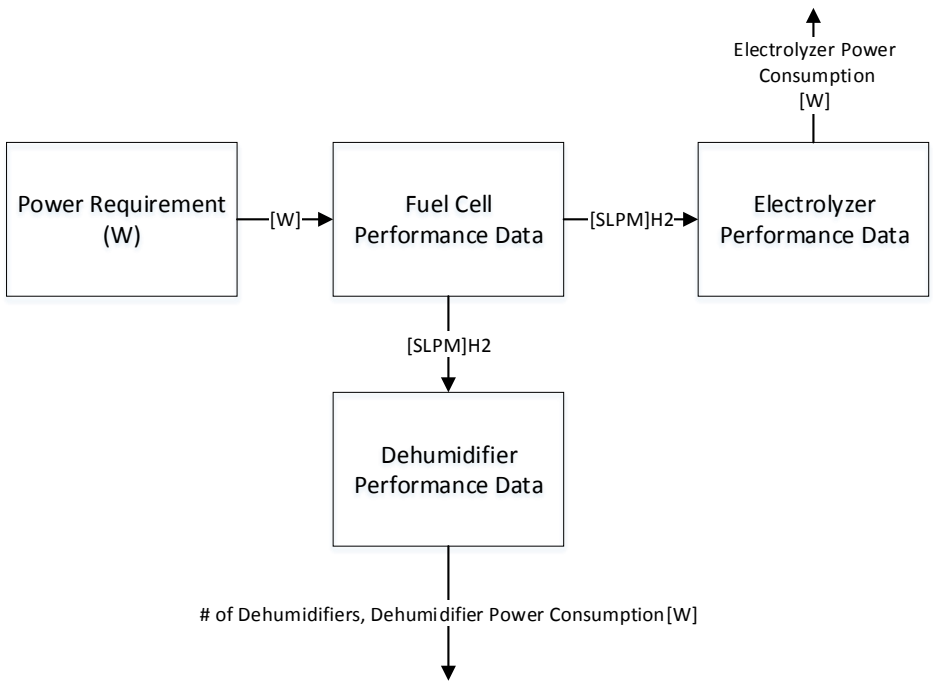

Figure 33. Power Efficiency Process

Once the power requirements were known, the efficiency of the system was calculated by using Equation 5. Because the fuel cell required 15 W of power for the fan, supply valve, and controller, it needed to be accounted for in the input power.

$$\eta = \frac{power\ out_{fuel\ cell}}{power\ in_{fuel\ cell} + power\ in_{electrolyzer} + power\ in_{dehumidifiers}} \qquad (5)$$

Figure 34 shows the system efficiency for cell fuel output ranging from 30 to 100 W. Notably, the system spends significantly more power on water production than on hydrogen production.

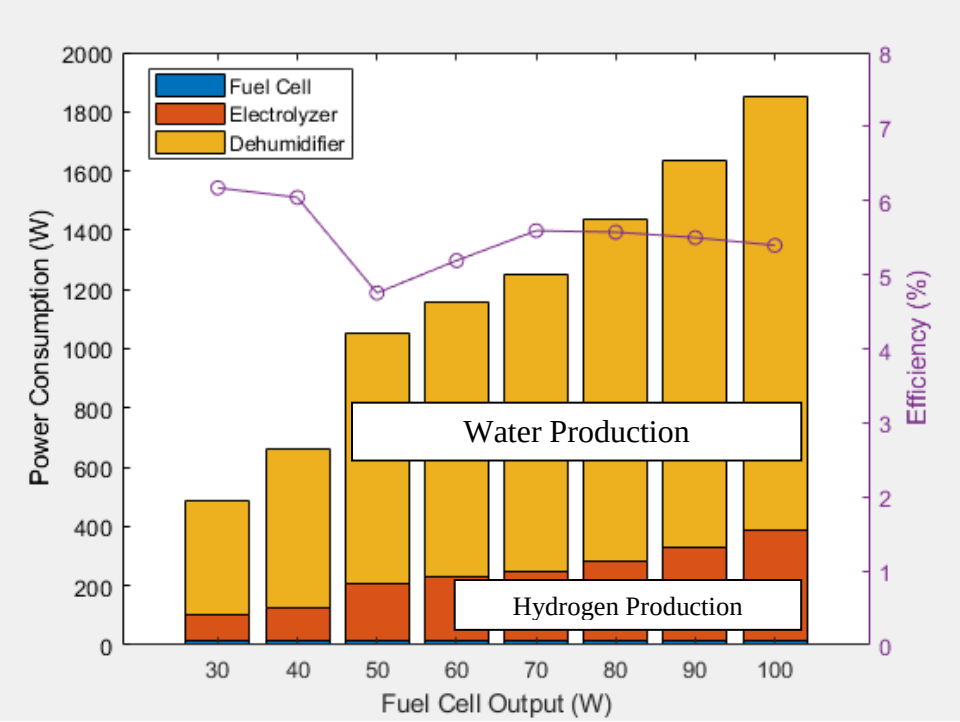

Figure 34. Power Efficiency

The power approach to system efficiency calculation assumed hydrogen was consumed by the fuel cell as it was produced by the electrolyzer. However, this was not how the system operated. Using solar power, the hydrogen was produced and stored for a later use instead of immediate consumption. The fuel cell was not needed when solar power was available for hydrogen production. Therefore, the system efficiency was more realistic if it were defined in terms of energy. For the energy approach, the desired output power by the fuel cell, the duration of the output, and hours of PV power available were needed. Based on the desired power output and the duration of the output, the total amount of hydrogen gas needed was calculated. Based on the total amount of hydrogen gas needed and hours of PV power available, the rate of hydrogen gas production was calculated. The rate of hydrogen gas production was then fed into the electrolyzer performance data to interpolate how much power was needed to produce desired hydrogen flow. The rate of hydrogen gas production was also fed into the dehumidifier performance data to calculate how many dehumidifiers were needed to produce enough water to satisfy the water demand for electrolysis. Based on the number of dehumidifiers,

the total power consumption of dehumidifiers was calculated. Figure 35 summarizes the process of how the energy requirement for the electrolyzer and dehumidifiers are determined based on fuel cell output power, the duration of the output, and the duration of PV power.

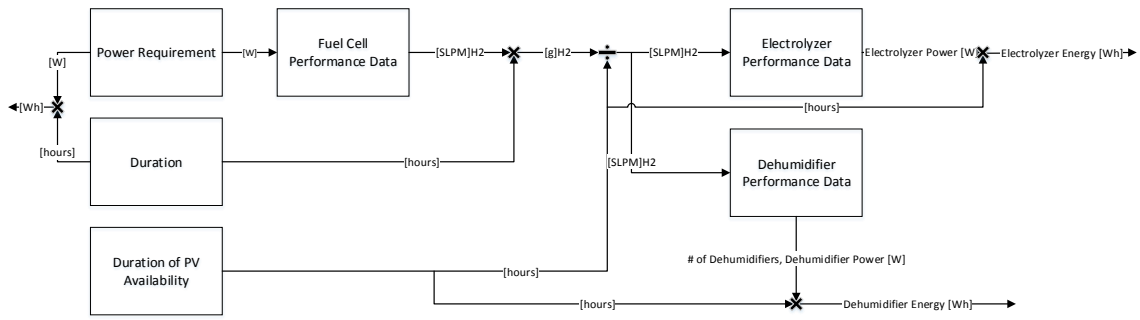

Figure 35. Energy Efficiency Process

Once the power requirements were known, the energy produced or consumed by each component was calculated by the timescale of production or consumption. The efficiency of the system was calculated by using Equation 6.

$$\eta = \frac{power\ out_{fuel\ cell} \times duration}{power\ in_{fuel\ cell} \times duration + (power\ in_{electrolyzer} + power\ in_{dehumidifiers}) \times PV\ hours} \quad (6)$$

Based on a power output of 12 hours and PV power availability of 8 hours, which were realistic operation parameters, Figure 36 shows the efficiency of the system for fuel cell output ranging from 30 to 100 W. Both the power and energy approach to the efficiency of the system yield similar results. However, the energy model assumes compression is not required and unlimited storage is available to store hydrogen gas at standard pressure and temperature. Due to the low density of hydrogen gas at standard temperature and pressure, this was not realistic. Therefore, the efficiency of the system using the energy approach will be lower when the work required to compress the hydrogen gas produced during day light hours is accounted for.

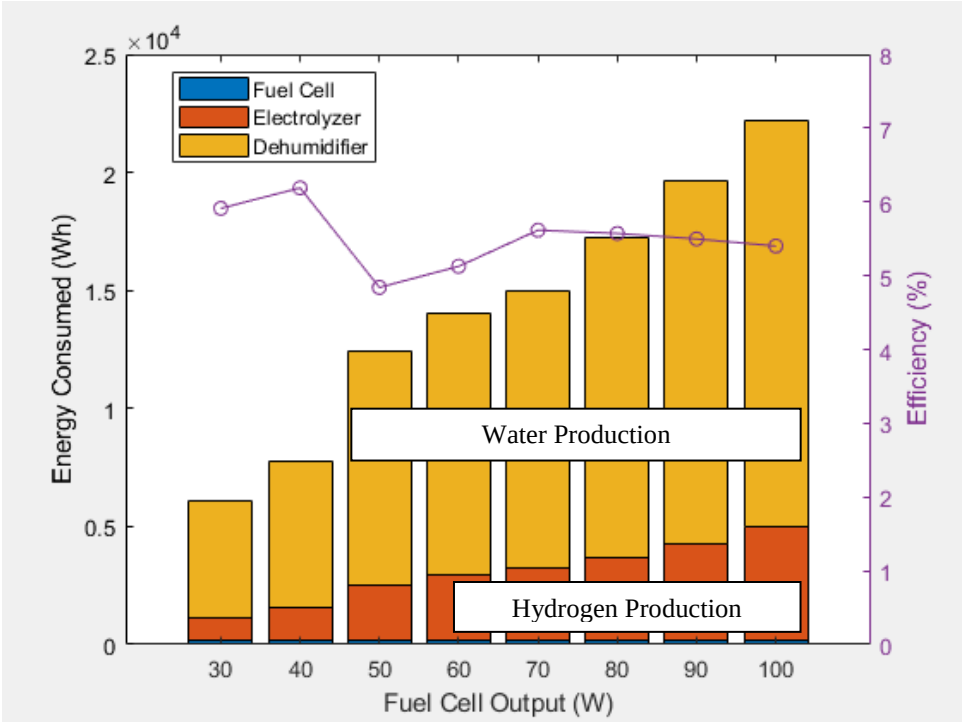

Figure 36. Energy Efficiency

E. SOLAR POWER TEST

After performance data was collected in a controlled environment with a power supply, the dehumidifiers and electrolyzer were tested with solar power to determine system performance in actual application. The test started at 0826 on November 1, 2017. Both dehumidifiers and the electrolyzer were powered by solar power. In the beginning of the experiment, there was enough solar power to run two of the four dehumidifiers. Figure 37 shows the results of the experiment without current control to the electrolyzer.

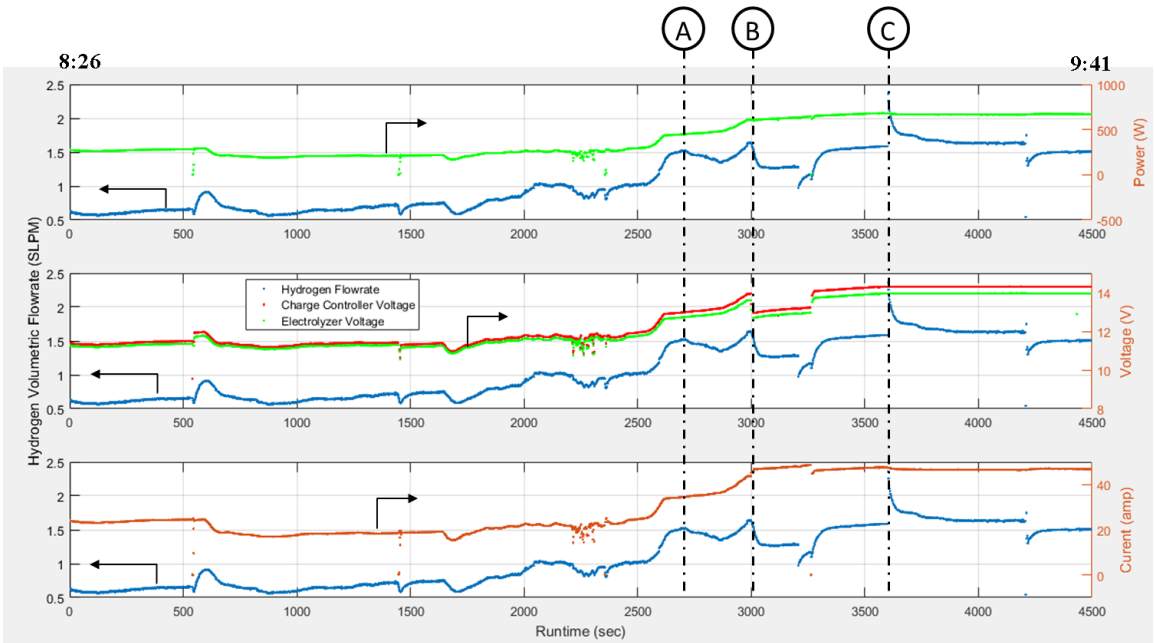

Figure 37. Hydrogen Production with Solar Power—without Electrolyzer Current Control

The hydrogen production changed as the solar power available changed except at times labeled A, B, and C. At time A, the decrease in hydrogen flowrate was due to the adjustment made to the needle valve that controlled the oxygen flowrate. As the solar power available increased, more hydrogen and oxygen were produced. The needle valve fixed the oxygen outlet area, which caused oxygen not leaving the system at the same rate as the hydrogen and to build up pressure in the oxygen electrolyte tank. This caused the electrolyte level to drop. Therefore, the needle valve was opened to increase oxygen flowrate and equalize the system pressure. By relieving the pressure on the oxygen tank, the hydrogen flowrate temporarily decreased due to the decrease in system pressure. At time B, all the dehumidifiers were turned on. As a result, less current was absorbed by the electrolyzer, even though the current being supplied to the entire system increased. The voltage of the electrolyzer also decreased due to the decrease in current, resulting in the decrease in hydrogen flowrate. Lastly, at time C, the high current supplied to the electrolyzer resulted in an electrolyzer voltage of 14 V and a charge controller voltage of 14.5 V. The high voltage supplied to the system caused the dehumidifiers to turn off because they were designed to operate between 11 and 13 V. After the dehumidifiers

were turned off, the current which flowing through the electrolyzer increased, which in turn increased the production of hydrogen. The needle valve was further opened to balance the system pressure. Because of the decrease in overall system pressure, this resulted in a decrease in hydrogen flowrate.

The charge controller treated the load connected to it as a battery since voltage supplied was always higher than the load voltage to push current through. As discussed earlier, the electrolyzer was the biggest load on the parallel circuit and dictated the system voltage. As seen in subplot 2 of Figure 37, the charge controller voltage was always higher than the electrolyzer voltage. The charge controller used MPPT to control the optimum voltage and current through the load based on available power. As power available increased, the voltage difference between the charge controller and the electrolyzer increased. The voltage of the electrolyzer varied based on the current going through the electrolyzer. As the solar power increased, the charge controller could send more current through the electrolyzer, which raised its voltage. Without current control to the electrolyzer, its voltage reached 14 V and the charge controller voltage was at 14.5 V. As a result, the dehumidifiers were automatically shut down due to overvoltage protection. The first experiment was concluded at 0941, so a Pulse Width Modular could be installed to control the current going through the electrolyzer to maintain a charge controller voltage of 13 V.

The experiment was resumed after a PWM was installed. The current going through the electrolyzer was set so that the electrolyzer voltage maintained at 12.5 V and the charge controller voltage was approximately 13 V. The results for the experiment with electrolyzer current control are shown in Figure 38. As expected, by controlling the current through the electrolyzer, the electrolyzer voltage was fixed at 12.5 V. However, the downside of controlling current to the electrolyzer was limiting hydrogen production and not utilizing all available solar power. However, this had to be done in order to operate the dehumidifiers and electrolyzer in the same circuit without a secondary voltage-controlling device to the dehumidifiers. The hydrogen production rate was for the most part constant. The small oscillations were due to system pressure imbalance and the need to modulate the oxygen needle valve. As the sun descended, the solar power

available decreased and voltage started to drop. The 4 instances near the end of the experiment in which the voltage dropped and subsequently went up were the result of turning off the dehumidifiers as solar power available decreased. The experiment concluded at 1735.

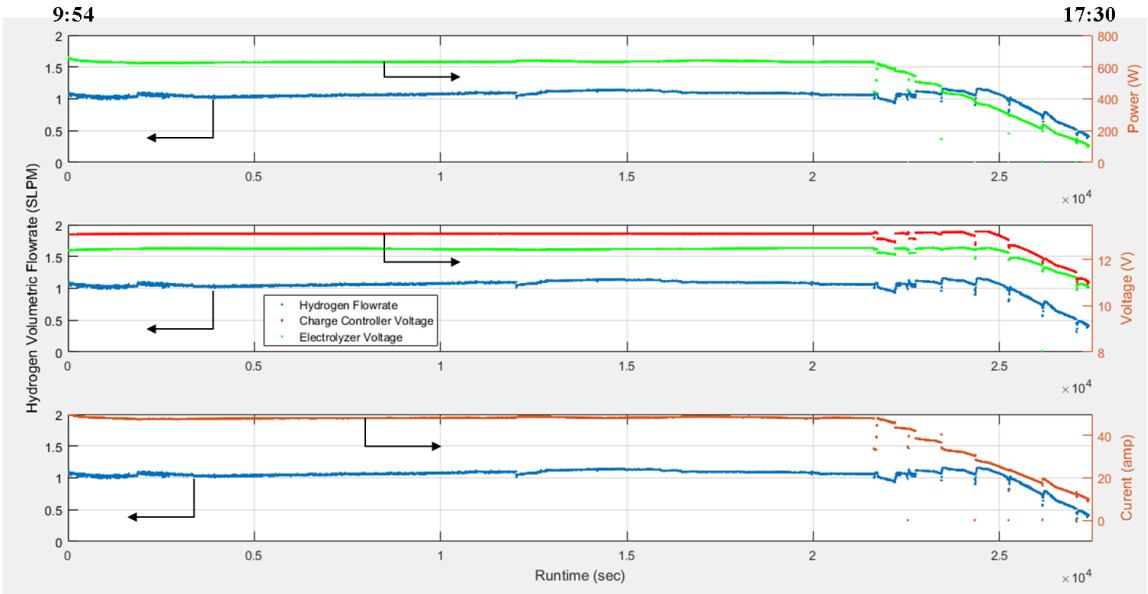

Figure 38. Hydrogen Production with Solar Power—with Electrolyzer Current Control

Using the voltage, current, and hydrogen volumetric flow rate data, the total amount of energy consumed and the amount of hydrogen produced were calculated. The water produced were measured at the end of the 2 experiments. All experimental results are shown in Table 5

Table 5. Solar Power Experimental Results

	Energy Used (Wh)	Hydrogen Produced (g)	Water Produced (g)
Experiment 1	502	6.63	90
Experiment 2	4387	39.38	
Total	4889	46.01	90

From the previous experiment, the fuel cell consumed 1.18 SLPM of hydrogen to produce 86.1 W of power to satisfy the load of the incandescent light bulb. Therefore, 46.01 g of hydrogen could be fed through the fuel cell to produce 679 Wh of energy and keep the light on for 7 hours and 53 minutes, which equated to an efficiency of 13.88%. However, the water produced was not enough to replenish the water consumed to produce hydrogen. For each gram of hydrogen gas produced, 8.936 g of water was required as shown in Appendix A. Therefore, to produce 46.01 g of hydrogen, 411 g of water was needed. In order to produce enough water, 14 more dehumidifiers would be needed in addition to the 4 existing dehumidifiers. More solar panels would be needed to support the power requirements of the extra panels and would reduce the efficiency.

Since the current going through the electrolyzer was limited and the dehumidifiers were consuming a fixed amount of power, it was assumed that all the available solar power was utilized. To confirm the assumption, the PVWatts Calculator developed by NREL was used. The specifications and location of the solar panels as well as the array tilt and azimuth were entered into PVWatts Calculator. By using historical solar irradiance data from local weather station, PVWatts Calculator provided the estimated array output on an hourly basis for an entire year. Since the experiment was conducted in November, the average hourly array output for November was plotted to compare with actual power used and shown in Figure 39. At the beginning and the end of the day, the actual power consumed closely matched the estimated power available. The available solar power during those times was limited and the system consumed all the power that was available. However, in the time between 1000 and 1600, excess power was not being utilized as suspected. An additional electrolyzer could be brought online to utilize the excess power and increase hydrogen production; or as mentioned earlier, additional dehumidifiers could also be added to the system.

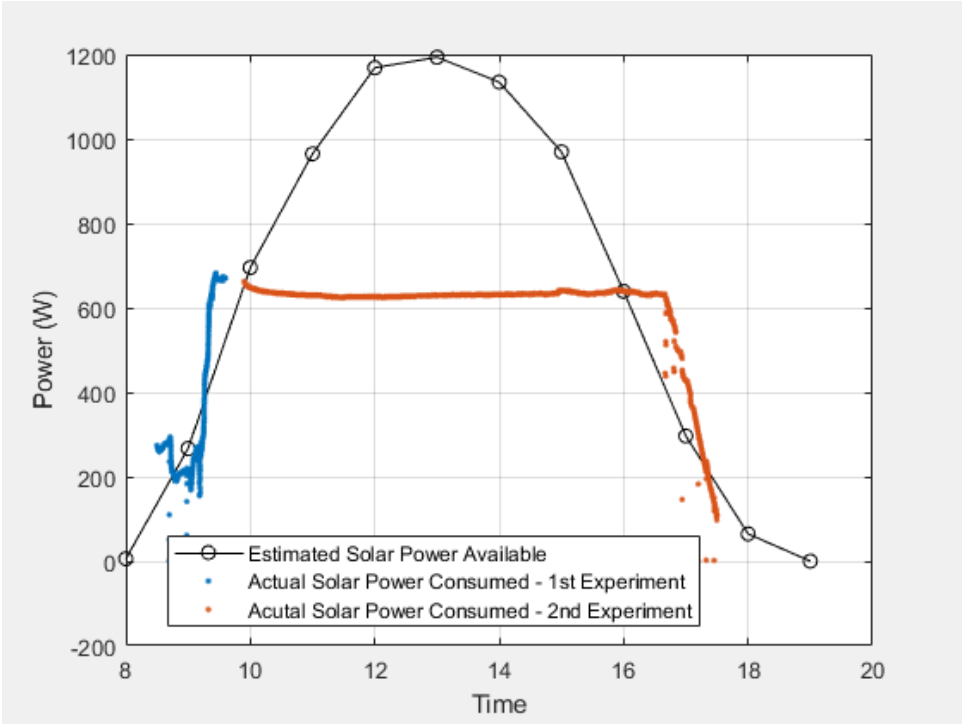

Figure 39. Solar Power Available and Solar Power Consumed

V. CONCLUSION

The purpose of this thesis was to implement a continuous data collection system to measure system performance data and improve system performance. Based on the data collected, a system deficiency was corrected to produce more continuous hydrogen and electric power with a hydrogen fuel cell. The data revealed that the oxygen flowrate needed to be controlled to maintain system pressure for continuous hydrogen production. A needle valve was installed at the oxygen outlet to control the oxygen flowrate. Once the needle valve was in place, the electrolyzer produced hydrogen continuously without causing a pressure imbalance.

As expected, the performance of the dehumidifier was most unpredictable. The amount of power drawn by each dehumidifier was constant. However, the amount of water produced or condensed by the dehumidifiers varied and was based on the ambient air's relative humidity. Based on the experimental results, 14 dehumidifiers would be needed to produce enough water to satisfy the water demand of the electrolyzer. Water production using dehumidification accounted for majority of the system energy consumption.

The electrolyzer demonstrated great flexibility in operating with intermittent power. As power available to the electrolyzer increased, the amount of hydrogen produced and vice versa. Similarly, the electrolyzer voltage increased as current supplied increased and vice versa. Therefore, in order to maintain a circuit voltage of 13 V, the current supplied to the electrolyzer needed to be controlled. In addition, as power supplied to the electrolyzer increased, the efficiency of the electrolyzer decreased. The efficiency ranged from 63% at low power input to 50% at the highest test power input. As a result, instead of having one electrolyzer operating at high power, multiple electrolyzers should be installed to operate at medium power to maintain system voltage as well as system efficiency.

The fuel cell was able to satisfy a full range of power requirements. However, similar to the electrolyzer, as the power output of the fuel cell increased, the efficiency

decreased. The efficiency of the fuel cell ranged from 65% at low power output to 48% at highest power output. In addition, the fuel cell short-circuited every 10 seconds for 100 milliseconds to recondition the cell and restore performance. This could be problematic for some equipment and would require a battery or capacitor to offset the power requirement during the short-circuit cycle. The short-circuit function could be disabled but the performance of the fuel cell degraded almost 17% in an hour.

The efficiency of the entire system ranged from 5 to 6% depending on the power output requirement of the fuel cell. The dehumidifiers consumed the most energy, accounted for 77.65% of the total energy consumed at the low end to 80.93% at the high end. The water production system presented a tremendous opportunity to improve the total system efficiency. Other methods of generating water should be investigated and considered.

Producing hydrogen using excess solar power proved successful. Unlike traditional electricity storage, hydrogen is much more versatile. Hydrogen can be used in a fuel cell as demonstrated in this thesis or combusted in a gas turbine to produce electricity. It can also be used in a drone to extend the range or in an internal combustion engine, for instance, weight handling equipment (WHE) to reduce carbon dioxide emissions in warehouses. Hydrogen can truly diversify DOD's energy portfolio and reduce dependence on fossil fuel.

VI. RECOMMENDATIONS

A. AUTOMATED CONTROL SYSTEM

An automated control system should be implemented to autonomously produce hydrogen when solar power is available. The automated control system would require at a minimum a controller, electrical relays, flow control valves, and water level sensors. The electrical relays would turn on and off the electrolyzer and dehumidifiers as power becomes available. The flow control valve would control the flow of oxygen based on the input from the water level sensors. The amount of hydrogen generated should also be tracked so the right amount of water can be added to the water reservoir to maintain the proper concentration of KOH.

B. OTHER WAYS OF WATER PRODUCTION

Because water production using dehumidification is energy intensive and unpredictable as to how much water can be produced on any given day, other ways of producing water should be investigated. In humid regions, water can be collected from existing HVAC condensation. The feasibility of using Ultra-violent light and carbon filters to remove micro-organism and particulate from the condensation stream should be investigated.

C. OTHER APPLICATION OF HYDROGEN

Because hydrogen is an energy carrier, besides fuel cells, other means of converting hydrogen into energy should be considered. Hydrogen can be combusted in a thermal engine or used to power a forklift. Hydrogen can also be used in drones to extend the range or fly time.

THIS PAGE INTENTIONALLY LEFT BLANK

APPENDIX A. CALCULATIONS

$H_2O \leftrightarrow H_2 + \frac{1}{2}O_2$

	M (g/mol)	ρ_{ref} (g/L)	LHV/ΔG (kJ/mol)
Water	18.015	1,000	237.2
Hydrogen	2.016	0.08235	241.8
Oxygen	31.999	1.4290	

Water consumption (g/min) per SLPM of hydrogen gas produced

$$1[SLPM]_{H_2} \times \rho_{H_2,ref}\left[\frac{g}{L}\right] \times M_{H_2}^{-1}\left[\frac{mol_{H_2}}{g}\right] \times \left[\frac{mol_{H_2O}}{mol_{H_2}}\right] \times M_{H_2O}\left[\frac{g}{mol_{H_2O}}\right]$$

$$= 0.08235 \times \left(\frac{1}{2.016}\right) \times 1 \times 18.015 = 0.7359\left[\frac{g}{\min}\right]_{H_2O}$$

Water required (g) per gram of hydrogen gas produced

$$1[g]_{H_2} \times M_{H_2}^{-1}\left[\frac{mol_{H_2}}{g}\right] \times \left[\frac{mol_{H_2O}}{mol_{H_2}}\right] \times M_{H_2O}\left[\frac{g}{mol_{H_2O}}\right]$$

$$= \left(\frac{1}{2.016}\right) \times 1 \times 18.015 = 8.936[g]_{H_2O}$$

SLPM of oxygen gas production per SLPM of hydrogen gas produced

$$1[SLPM]_{H_2} \times \rho_{H_2,ref}\left[\frac{g}{L}\right] \times M_{H_2}^{-1}\left[\frac{mol_{H_2}}{g}\right] \times \frac{1}{2}\left[\frac{mol_{O_2}}{mol_{H_2}}\right] \times M_{O_2}\left[\frac{g}{mol_{O_2}}\right] \times \rho_{O_2,ref}^{-1}\left[\frac{L}{g}\right]$$

$$= 0.08235 \times \left(\frac{1}{2.016}\right) \times \frac{1}{2} \times 31.999 \times \left(\frac{1}{1.4290}\right) = 0.4573[SLPM]_{O_2}$$

Convert hydrogen volumetric flowrate to power using LHV of hydrogen

$$[SLPM]_{H_2} \times \rho_{H_2}\left[\frac{g}{L}\right] \times M_{H_2}^{-1}\left[\frac{mol}{g}\right] \times LHV_{H_2}\left[\frac{kJ}{mol}\right] \times \frac{1}{60}\left[\frac{\min}{\sec}\right] \times 1{,}000\left[\frac{J}{kJ}\right] = \left[\frac{J}{\sec}\right] = [W]$$

THIS PAGE INTENTIONALLY LEFT BLANK

APPENDIX B. MATLAB CODE

```
clear all;close all;clc;
% Establish connection with measurement devices prior to running data
collection code

%% FuelCell + Eletrolyzer
flowMeter=serial('COM6','TimeOut',2,'BaudRate',19200,'Terminator','CR')
;
amp_out=serial('COM9');
volt_out=serial('COM8');
amp_in=serial('COM7');
fopen(flowMeter);
fopen(amp_out);
fopen(volt_out);
fopen(amp_in);

%% Electrolyzer
volt_in=serial('COM8');
fopen(volt_in);
amp_in=serial('COM7');
fopen(amp_in);
flowMeter=serial('COM6','TimeOut',2,'BaudRate',19200,'Terminator','CR')
;
fopen(flowMeter);

%% Dehumidifier
volt_in=serial('COM8');
fopen(volt_in);
amp_in=serial('COM7');
fopen(amp_in);
```

```
% code for measuring power input to the dehumidifier

samplerate=1;   %sampling rate, 1=1 sample every second
n=90000;        %# of samples to collect data for

for i=1:n
    tic
    timerecord(i)=now;
    fprintf(amp_in,'READ?');
    current(i)=str2double(fscanf(amp_in));
    fprintf(volt_in,'READ?');
    volt(i)=str2double(fscanf(volt_in));
%     plot(i,volt(i),'p',i,current(i),'o');
%     grid on;xlabel('Runtime (sec)');ylabel('Input (Voltage &
Current)');
%     hold on;
    pause(samplerate-toc)

end
```

```
% code for meauring power input and flowrate of hydrotube
samplerate=1;     %sampling rate, 1=1 sample every second
n=10000;          %# of samples to collect data for

for i=1:n
    tic
    timerecord(i)=now;
    fprintf(flowMeter,'A');
    IN=fscanf(flowMeter);

[OUT.ID,OUT.pressure,OUT.temp,OUT.LPM,OUT.SLPM,OUT.gas]=strread(IN,'%s%
f%f%f%f%s', 'delimiter', ' ');
    flowrate_H_slpm(i)=OUT.SLPM;
    flowrate_H_lpm(i)=OUT.LPM;
    pressure_H(i)=OUT.pressure;
    temp_H(i)=OUT.temp;
    fprintf(flowMeter,'B');
    IN=fscanf(flowMeter);

[OUT.ID,OUT.pressure,OUT.temp,OUT.LPM,OUT.SLPM,OUT.gas]=strread(IN,'%s%
f%f%f%f%s', 'delimiter', ' ');
    flowrate_O_slpm(i)=OUT.SLPM;
    flowrate_O_lpm(i)=OUT.LPM;
    pressure_O(i)=OUT.pressure;
    temp_O(i)=OUT.temp;
    fprintf(amp_in,'READ?');
    current(i)=str2double(fscanf(amp_in));
    fprintf(volt_in,'READ?');
    voltage(i)=str2double(fscanf(volt_in));
    plot(i,flowrate_H_lpm(i),'hb',i,flowrate_O_lpm(i),'og');  %plot
data as being collected
    grid on;xlabel('Sample #');ylabel('Flowrate
(LPM)');legend('Hydrogen','Oxygen');
    hold on;
    pause(samplerate-toc)

end
```

```
% code for measuring power input, power output, and hydrogen flow rate
to fuel cell
% oxygen flow rate is also meausred to compare fuel cell performance
with
% oxygen injection

samplerate=1;   %sampling rate, 1=1 sample every second
n=90000;        %# of samples to collect data for

for i=933:n
    tic
    timerecord(i)=now;
    fprintf(flowMeter,'A');
    IN=fscanf(flowMeter);

[OUT.ID,OUT.pressure,OUT.temp,OUT.LPM,OUT.SLPM,OUT.gas]=strread(IN,'%s%
f%f%f%f%s', 'delimiter', ' ');
    flowrate_H_slpm(i)=OUT.SLPM;
    flowrate_H_lpm(i)=OUT.LPM;
    pressure_H(i)=OUT.pressure;
    temp_H(i)=OUT.temp;
    fprintf(flowMeter,'B');
    IN=fscanf(flowMeter);

[OUT.ID,OUT.pressure,OUT.temp,OUT.LPM,OUT.SLPM,OUT.gas]=strread(IN,'%s%
f%f%f%f%s', 'delimiter', ' ');
    flowrate_O_slpm(i)=OUT.SLPM;
    flowrate_O_lpm(i)=OUT.LPM;
    pressure_O(i)=OUT.pressure;
    temp_O(i)=OUT.temp;
    fprintf(amp_out,'READ?');
    current_out(i)=str2double(fscanf(amp_out));
    fprintf(volt_out,'READ?');
    voltage_out(i)=str2double(fscanf(volt_out));
    fprintf(amp_in,'READ?');
    current_in(i)=str2double(fscanf(amp_in));
    power(i)=current_out(i)*voltage_out(i);
    plot(flowrate_H_lpm(i),power(i),'p');  %plot data as being
collected
    grid on;xlabel('Hydrogen Flowrate (LPM)');ylabel('Power Out (W)');
    ylim([0 100]);
    hold on;
    pause(samplerate-toc)
end
```

APPENDIX C. DETAILED EXPERIMENTAL ELECTROLYZER RESULTS

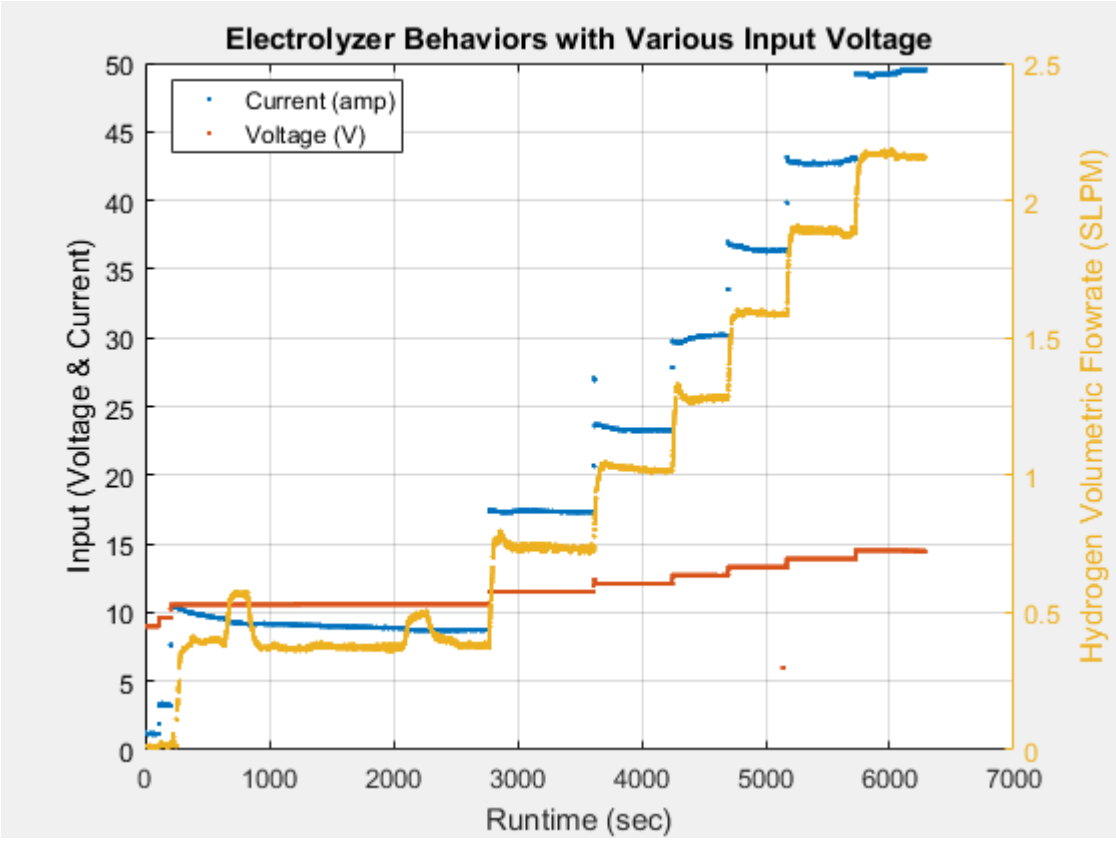

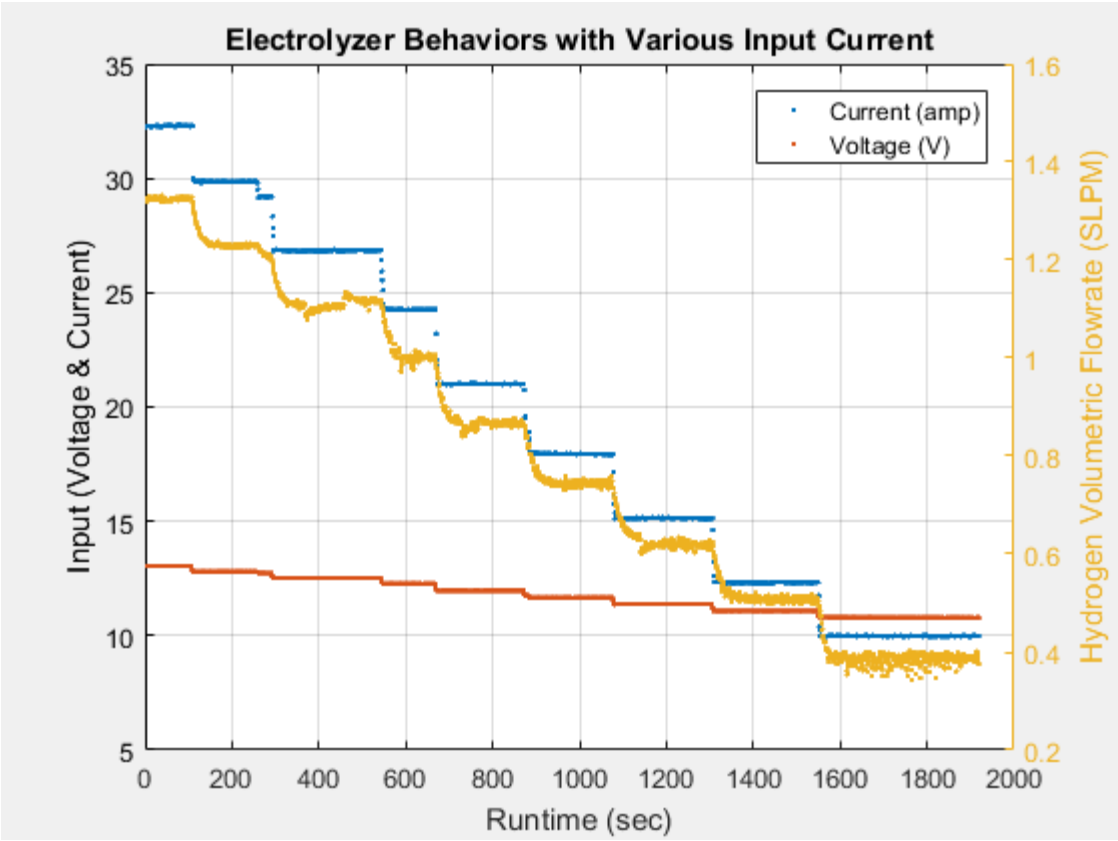
Electrolyzer Behaviors with Various Input Current
Current (amp)
Voltage (V)
Input (Voltage & Current)
Hydrogen Volumetric Flowrate (SLPM)
Runtime (sec)
35
30
25
20
15
10
5
1.6
1.4
1.2
1
0.8
0.6
0.4
0.2
0
200
400
600
800
1000
1200
1400
1600
1800
2000

APPENDIX D. ELECTRICAL DIAGRAM

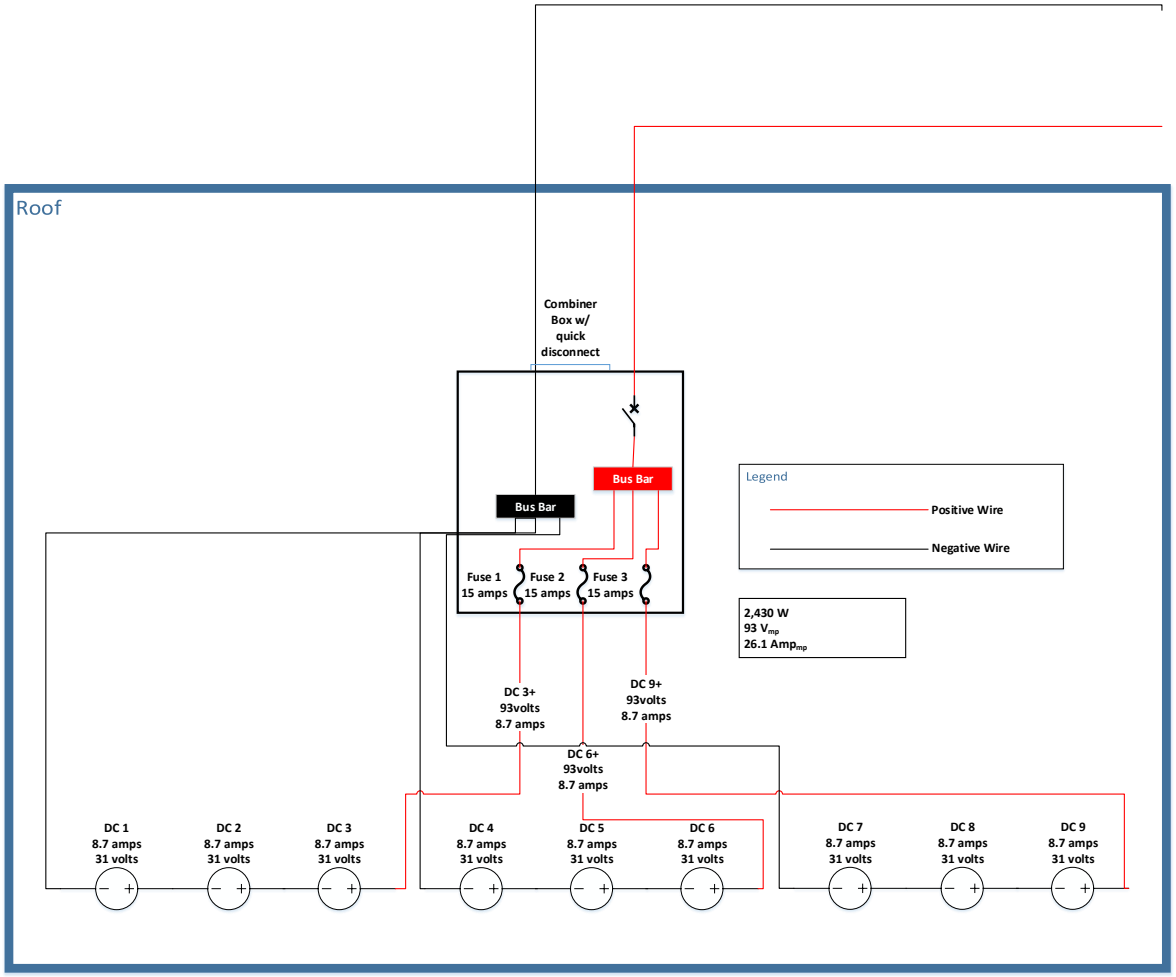

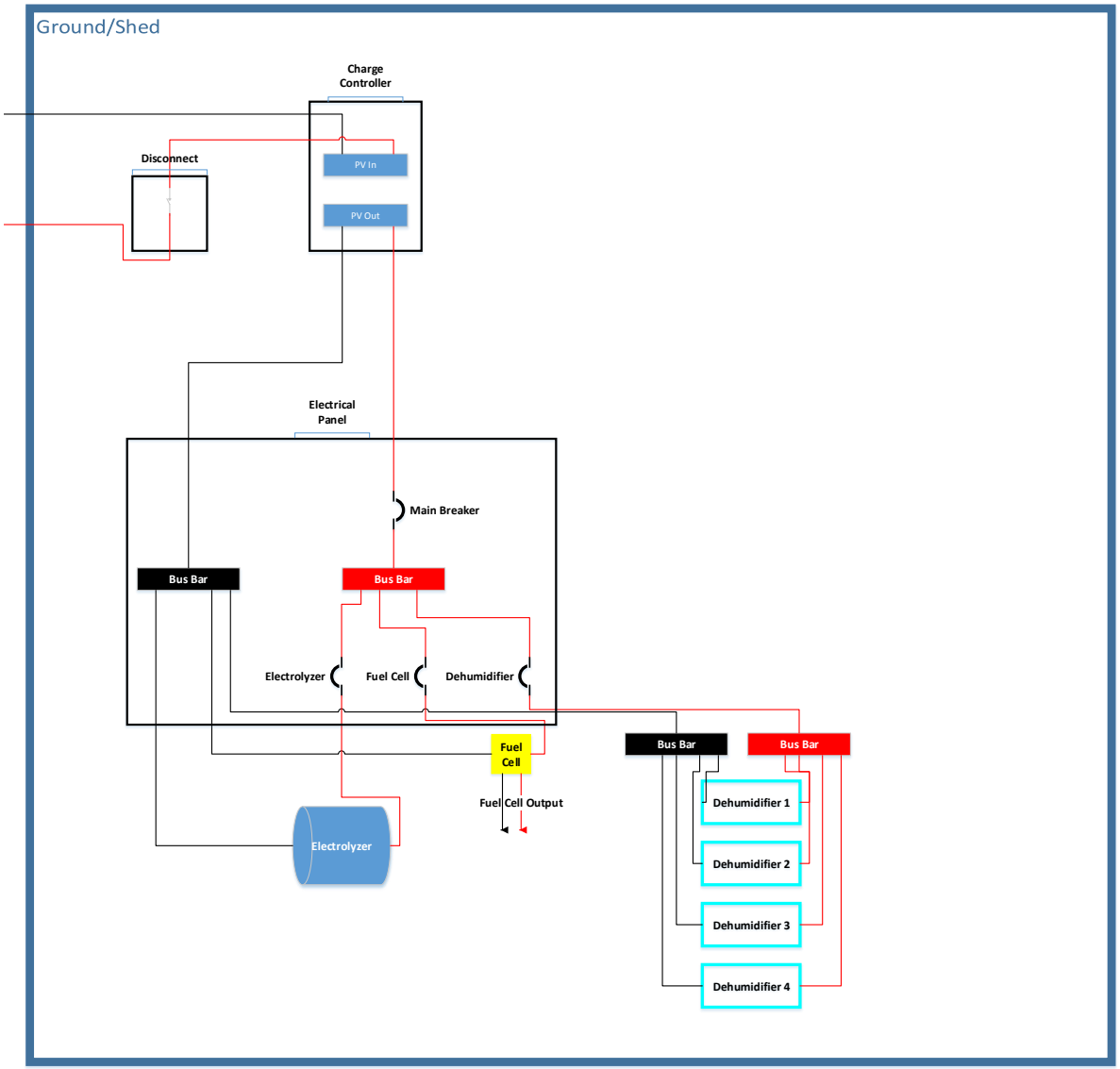
Ground/Shed
Charge Controller
PV In
PV Out
Disconnect
Electrical Panel
Main Breaker
Bus Bar
Bus Bar
Electrolyzer
Fuel Cell
Dehumidifier
Fuel Cell
Fuel Cell Output
Electrolyzer
Bus Bar
Bus Bar
Dehumidifier 1
Dehumidifier 2
Dehumidifier 3
Dehumidifier 4

APPENDIX E. MECHANICAL DIAGRAM

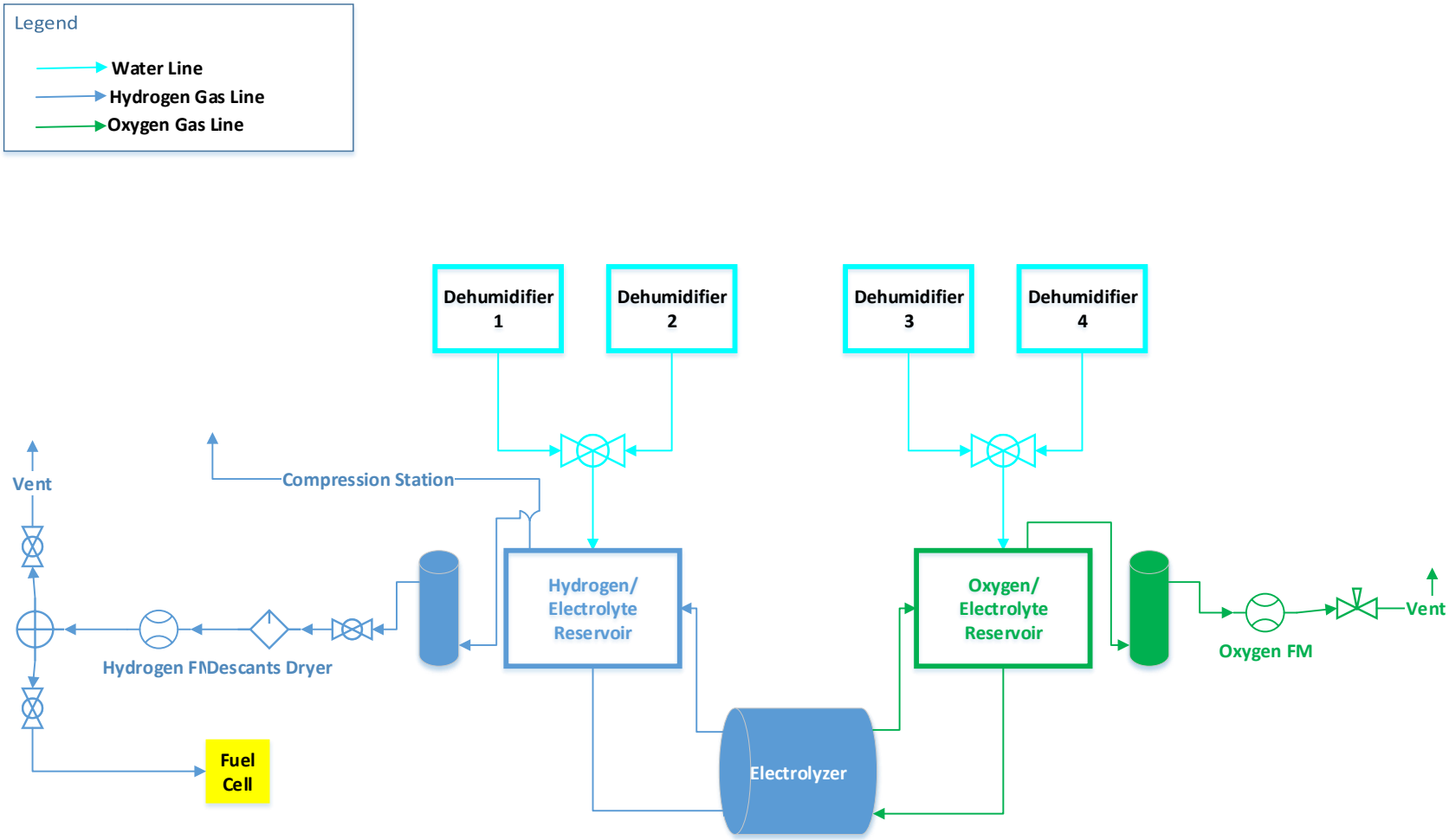

THIS PAGE INTENTIONALLY LEFT BLANK

LIST OF REFERENCES

[1] Alexander, Sun. "Monthly Energy Review—April 2017." Report No. DOE/EIA-0035(2017/4). U.S. Energy Information Administration, Washington, DC. 2017.

[2] Castillo, Ariel and Brown, Joshua. "Department of Defense Annual Energy Management Report—Fiscal Year 2015." RefID: 3–4DBD001, Office of the Assistant Secretary of Defense, Washington, DC. 2016.

[3] Council on Foreign Relations, "A Cyberattack on the U.S. Power Grid." URL https://www.cfr.org/report/cyberattack-us-power-grid

[4] Marqusee, Jeffrey and Schultz, Craig. "Power Begins at Home: Assured Energy for U.S. Military Bases." The Pew Charitable Trusts, Philadelphia, PA. 2017.

[5] Lazard, "Lazard's Levelized Cost of Energy Analysis 10.0." Lazard. 2016. URL https://www.lazard.com/perspective/levelized-cost-of-energy-analysis-100/

[6] LaRose, Angelina. "Annual Energy Outlook 2017." Report No. AEO2017. U.S. Energy Information Administration, Washington, DC. 2017.

[7] OhmHome, "2016 Solar Penetration by State." URL https://www.ohmhomenow.com/2016-solar-penetration-state/

[8] *Los Angeles Times*. "California invested heavily in solar power. Now there's so much that other states are sometimes paid to take it." URL http://www.latimes.com/projects/la-fi-electricity-solar/

[9] Denholm, Paul., Ela, Erik., Kirby, Brenda and Miligan, Michael. "The Role of Energy Storage with Renewable Electricity Generation." Technical Report No. NREL/TP-6A2-47187. NREL, Golden, CO. 2010.

[10] Hart, David and Sarkissian, Alfred. "Deployment of Grid-Scale Batteries in the United States." George Mason University, Fairfax, VA. 2016.

[11] Carnegie, Rachel., Gotham, Douglas., Nderitu, David and Preckl, Paul "Utility Scale Energy Storage Systems." State Utility Forecasting Group, West Lafayette, IN. 2013.

[12] Energy Storage Association. "Compressed Air Energy Storage (CAES)." URL http://energystorage.org/compressed-air-energy-storage-caes

[13] Eichman, Josh and Marc, Melaina "Hydrogen Energy Storage: Grid and Transportation Services." Technical Report No. NREL/TP-5400-62518. NREL, Golden, CO. 2015.

[14] Aviles, Angel. “Renewable Production of Water, Hydrogen, and Power from Ambient Moisture.” Master Thesis. Naval Postgraduate School, Monterey, CA. 2016.

[15] Lindeburg, Michael. *Mechanical Engineering Reference Manual for the PE Exam Thirteen Edition.* Professional Publications, Belmont, CA (2013).

[16] Martin-Gomez, Cesar. “Thermoelectric cooling heating unit prototype.” *Thermoelectric cooling* Vol.37 No.4 (2016): pp.431-449.

[17] Zeng, Kai and Zhang, Dongke. “Recent Progress in Alkaline Water Electrolysis for Hydrogen Production and Applications,” *Progress in Energy and Combustion Science* Vol. 36 No. 3 (2010): pp207-326.

[18] Godula-Jopek, Agata. *Hydrogen Production by Electrolysis.* Wiley, Hoboken (2015).

[19] Bazant, Martin. “Theory of Electrochemical Kinetics based on Nonequilibrium Thermodynamics.” Massachusetts Institute of Technology, Cambridge, MA. 2013.

[20] Larmine, James and Dicks, Andrew. *Fuel Cell Systems Explained 2nd Edition*. John Wiley & Sons, England (2003).

[21] *NEC 2014: NFPA 70 National electrical code*. National Fire Protection Association, Quincy, MA (2014).

[22] Benziger, Jay. “The power performance curve for engineering analysis of fuel cells.” Princeton University, Princeton, NJ. 2005.

[23] Office of Energy Efficiency & Renewable Energy. “DOE Technical Targets for Hydrogen Production from Electrolysis.” URL https://energy.gov/eere/fuelcells/doe-technical-targets-hydrogen-production-electrolysis

[24] Ale, Bhakta Bahadur and Shrestha, Bade. “Experimental Study on Performance Characteristics of a PEM Fuel Cell.” *Journal of the Institute of Engineering* Vol. 7 No. 1 (2009): pp31-39.

INITIAL DISTRIBUTION LIST

1. Defense Technical Information Center
   Ft. Belvoir, Virginia

2. Dudley Knox Library
   Naval Postgraduate School
   Monterey, California